Soluble theories for the density of states of a spatially disordered two-level tight-binding model

1989 J. Phys.: Condens. Matter 1 8683

(http://iopscience.iop.org/0953-8984/1/44/038)

J. Phys.: Condens. Matter **1** (1989) 8683–8708. Printed in the UK

Soluble theories for the density of states of a spatially disordered two-level tight-binding model

Martyn D Winn and David E Logan
Physical Chemistry Laboratory, University of Oxford, South Parks Road, Oxford OX1 3QZ, UK

Received 31 May 1989

Abstract. An analysis is given for the configurationally averaged Green functions of a random multi-level tight-binding model characterised by quenched liquid-like disorder, using graph-theoretical methods. An exact self-consistency equation for the average diagonal Green function matrix, $\bar{\mathbf{G}}(z)$, is derived, from which follow the partial densities of states (DOS). From the exact description, various approximate theories for $\bar{\mathbf{G}}(z)$ may be developed systematically. We examine in particular three tractable theories for the case of a two-band system: the Hubbard approximation, the Matsubara–Toyozawa approximation and the single super-chain approximation (SSCA) which is equivalent to the effective medium approximation (EMA) of Roth. With Yukawa transfer matrix elements the SSCA/EMA is solved analytically by exploiting direct analogies with the theory of classical binary liquid mixtures. For all three theories the material parameter dependence of the DOS is examined systematically and comparatively, with particular regard to band overlap effects which may lead to a metal–insulator transition.

1. Introduction

A detailed understanding of the electronic properties of liquids and amorphous solids is in many ways still in its infancy. Even at an idealised one-electron level of description, where the numerous facets of electron–electron interactions are ignored, the role of disorder must be taken seriously and can lead to profound effects such as disorder-induced localisation. From the viewpoint of a solid-state theorist, and granted even a one-electron description, the problem of dealing with spatially disordered systems is particularly acute due to the absence of an underlying periodicity characteristic of crystalline materials. Theories for even the simplest quantities characteristic of spatially disordered systems, such as the density of states (DOS), are often computationally arduous and somewhat unsystematic in construct.

Liquid-state theory can, however, help here. Recently, for example, an exact analysis has been given (Logan and Winn 1988, hereafter referred to as I) for the configurationally averaged Green functions of a one-band tight-binding model characterised by quenched liquid-like disorder, using a graph-theoretical analysis originally applied by Wertheim (1973) to a problem in the classical dielectric theory of fluids. The essential equation governing the structure of the averaged Green functions was found to be formally equivalent to the Ornstein–Zernike equation for the pair distribution function of a classical liquid. From this, by exploiting additional parallels in liquid-state theory,

0953-8984/89/448683 + 26 $02.50

approximate theories for the DOS can be constructed systematically. This was examined further by Winn and Logan (1989, hereafter referred to as II) who developed in particular an approximate single-site theory for the DOS, the single super-chain approximation (SSCA). Although formulated differently, it was shown in II that the SSCA is equivalent to the well known effective medium approximation (EMA) due to Roth (1974, 1976).

The manner in which the SSCA is formulated leads to another connection with conventional liquids theory: for a simple model pair distribution function characterising the disordered system, the EMA/SSCA for the averaged Green function was shown in II to be mathematically equivalent to the mean spherical approximation for the pair distribution function of a classical liquid. This correspondence in turn leads to the possibility of analytical solutions to the SSCA/EMA, which were given in II for the particular case of a Yukawa transfer matrix element. Subsequent computer simulations by Bush *et al* (1989a) have shown that this simple analytical theory gives a good description of the DOS over a substantial range of reduced densities. We note too that recent related work by Stratt and Xu (1989a, b) has also demonstrated clearly, by different methods, how techniques of liquid-state theory can aid in developing computationally tractable theories for the averaged Green functions of topologically disordered systems.

Most theoretical work on the electronic properties of liquids and amorphous solids, at the tight-binding level, has focused on a one-band tight-binding model with a single unperturbed level associated with each site. While such a model is relevant to tightly bound bands in certain liquid metals, alloys and doped semiconductors, it is clearly somewhat restrictive. For many non-simple disordered systems (such as noble and transition metals) several different bands, some of which may be degenerate, are important in determining electrical properties, particularly when a metal–insulator transition stems from valence/conduction band overlap together with the localising effects of disorder, as perhaps occurs in divalent liquid metals.

In this paper we seek to extend the theory of I and II for the averaged Green functions to the case of a multi-level per site tight-binding model. Some work has been done on this problem, particularly by Yonezawa and co-workers (Yonezawa and Martino 1976, Yonezawa *et al* 1977) for the specific case of liquid Hg. Our aim here is to develop a formally exact description of the problem, and to investigate systematically and comparatively different approximate but tractable theories for the DOS. As in I and II, this is achieved by building on parallels to classical liquid-state theory. Section 2 (and the beginning of § 3) contains the formal theory; a self-consistency equation is derived for the averaged diagonal Green functions (from which follow the partial DOS), and we find that the basic equation governing the averaged off-diagonal Green function for an n-level tight-binding model is closely related to the Ornstein–Zernike equation for a classical n-component liquid mixture. In § 3 some general features of the exact theory are discussed, and we start to examine tractable theories for the DOS beginning with the Hubbard approximation which, although simplistic, brings out many features of more sophisticated theories. Although most of the formal theory we develop is applicable to a general n-level system, specific approximate theories are for simplicity investigated for the simple case of a two-level system with Yukawa (modified exponential) transfer matrix elements.

Section 4 contains a brief general discussion of single-site theories for the DOS, followed by an analysis of the Matsubara–Toyozawa (1961) approximation (MTA) applicable to a perfectly random system where the effects of short-ranged structural correlations are neglected. In § 5 we investigate the two-level SSCA/EMA, which is believed to be the most accurate single-site theory for the DOS. As in II, and by exploiting Blum

and Høye's (1978) solution to the mean spherical approximation for a binary liquid mixture, we obtain solutions to the SSCA/EMA for the DOS. Section 6 contains a brief discussion of the incorporation of site-diagonal disorder into the problem; for any single-site theory this requires only minor modification of the present work.

Finally, we comment on two additional motivations for this work. First, granted a one-electron (or effective one-electron) level of description, we would like ultimately to investigate the role of Anderson localisation occurring in a pseudogap formed from overlapping bands, a mechanism of possible relevance to the metal–insulator transition occurring in divalent liquid metals. Although a theory of localisation in such systems is considerably more subtle than calculation of averaged Green functions, a knowledge of the DOS is an essential ingredient in such a theory. Second, in a regime of weak disorder where states at the Fermi energy are sufficiently extended, a knowledge of the averaged Green functions (both diagonal and off-diagonal) is sufficient to provide a reasonable estimate of the electrical conductivity.

2. Green function formalism and topological reductions

For a given realisation the model system we consider is specified by a tight-binding Hamiltonian

$$H = \sum_i \sum_\alpha \varepsilon_{i_\alpha} c_{i_\alpha}^+ c_{i_\alpha} + \sum_{i,j}{}' \sum_{\alpha,\beta} V_{ij}^{\alpha\beta} c_{i_\alpha}^+ c_{j_\beta}. \tag{1}$$

$c_{i_\alpha}^+$ (c_{i_α}) is a creation (annihilation) operator for the one-electron (or exciton) state associated with level α on site i, which has centre of mass position $\boldsymbol{R}_i$. ε_{i_α} is the zero-order site energy of level α, and $V_{ij}^{\alpha\beta}$ is the transfer matrix element between level α on site i and level β on site j. The sums in (1) run over all N sites and n levels, and the prime in the second site summation excludes the case $j = i$. The ε_{i_α} may be regarded as independent random variables with a given probability distribution $P(\{\varepsilon_{i_\beta}\})$ for any site, but to begin with we will neglect site-diagonal disorder and take $\varepsilon_{i_\alpha} = \varepsilon_\alpha$ for all i; incorporation of site-diagonal disorder within the framework of any single-site approximation to the averaged Green function is straightforward, and will be discussed briefly in § 6. We will also assume that $V_{ij}^{\alpha\beta}$ depends only on α, β and the relative site centre-of-mass separation, $V_{ij}^{\alpha\beta} \equiv V^{\alpha\beta}(\boldsymbol{R}_i - \boldsymbol{R}_j)$; randomness in the transfer matrix elements thus arises solely from the spatial disorder.

For a given realisation of the random system the Green function $G_{ij}^{\alpha\beta}(z)$, defined by

$$G_{ij}^{\alpha\beta}(z) = \langle 0|c_{i_\alpha}(z - H)^{-1} c_{j_\beta}^+|0\rangle \tag{2}$$

(where $|0\rangle$ is the vacuum state and $z = E + \mathrm{i}\eta$ ($\eta \to 0+$) is the energy), satisfies

$$(z - \varepsilon_{i_\alpha}) G_{ij}^{\alpha\beta}(z) - \sum_k{}' \sum_\gamma V_{ik}^{\alpha\gamma} G_{kj}^{\gamma\beta}(z) = \delta_{ij}\delta_{\alpha\beta}. \tag{3a}$$

This equation has the formal solution

$$G_{ij}^{\alpha\beta}(z) = [(\tilde{\mathbf{Z}} - \mathbf{V})^{-1}]_{ij}^{\alpha\beta} \tag{3b}$$

where $\mathbf{V}$ and $\tilde{\mathbf{Z}}$ are $N \times N$ matrices with elements that are themselves $n \times n$ matrices such that $[\mathbf{V}]_{ij}^{\alpha\beta} = V_{ij}^{\alpha\beta}$ and $[\tilde{\mathbf{Z}}]_{ij}^{\alpha\beta} = (z - \varepsilon_{i\alpha})\delta_{ij}\delta_{\alpha\beta}$ ($[\tilde{\mathbf{Z}}]_{ij}^{\alpha\beta}$ refers to the (α, β) element of the (i, j) element of a matrix). We are here interested in the ensemble-averaged Green

functions. The ensemble average of any function, f, which depends on the centres of mass and site energies of any number $M \leq N$ of sites is defined by

$$\langle f \rangle = Z_N^{-1} \int \ldots \int \prod_{i=1}^{N} \prod_{\alpha=0}^{n-1} [\mathrm{d}\boldsymbol{R}_i \, \mathrm{d}\varepsilon_{i\alpha} P(\{\varepsilon_{i\beta}\})] f \exp(-\beta \Phi_N(\boldsymbol{R}^N)). \tag{4}$$

Here $\beta = 1/kT$ and Z_N is the configurational integral for a system of N particles interacting via $\Phi_N(\boldsymbol{R}^N)$, where $\boldsymbol{R}^N$ denotes collectively the site centre-of-mass positions. Φ_N embodies explicitly the liquid-like structure of the disordered medium. Although it is often convenient to treat Φ_N as a sum of pairwise-additive potentials, this is not a necessary restriction, and in what follows Φ_N may include many-body terms.

The Green functions can clearly be diagonal in both site and level indices, but in what follows the term 'diagonal Green function' refers solely to the site indices. The ensemble-averaged diagonal Green function is thus given by

$$\bar{G}^{\alpha\beta}(z) = \langle G_{ii}^{\alpha\beta}(z) \rangle \tag{5a}$$

and the averaged density of states (DOS) associated with level α is obtained from:

$$D_\alpha(E) = -\pi^{-1} \operatorname{Im} \bar{G}^{\alpha\alpha}(E + \mathrm{i}\eta). \tag{5b}$$

Performing an ensemble average of equation (3a) for the case $j = i$, using equation (4) with $P(\{\varepsilon_{i\alpha}\}) = \prod_\alpha \delta(\varepsilon_{i\alpha} - \varepsilon_\alpha)$, and noting that the system is translationally invariant on average, we find

$$z_\alpha \bar{G}^{\alpha\beta}(z) = \delta_{\alpha\beta} + \rho \sum_\gamma \int \mathrm{d}\boldsymbol{R}' V^{\alpha\gamma}(\boldsymbol{R} - \boldsymbol{R}') \bar{G}^{\gamma\beta}(\boldsymbol{R}' - \boldsymbol{R}). \tag{6a}$$

Here $z_\alpha = z - \varepsilon_\alpha$, and $\bar{G}^{\alpha\beta}(\boldsymbol{R}' - \boldsymbol{R})$ is the ensemble-averaged off-diagonal Green function defined by

$$\rho^2 \bar{G}^{\alpha\beta}(\boldsymbol{R} - \boldsymbol{R}') = \Big\langle \sum_{i,j}{}' G_{ij}^{\alpha\beta} \delta(\boldsymbol{R}_i - \boldsymbol{R}) \delta(\boldsymbol{R}_j - \boldsymbol{R}') \Big\rangle. \tag{6b}$$

$\rho = N/V$ is the number density of sites, where V is the volume of the system. Note that $\bar{G}^{\alpha\beta}(\boldsymbol{0}) = 0$, reflecting the fact that $\Phi_N \to \infty$ as $(\boldsymbol{R}_i - \boldsymbol{R}_j) \to \boldsymbol{0}$.

Equations (6), together with (3b) and the defined averaging procedure, form the starting point for an exact analysis of the averaged Green functions for a multi-level per site system, using the methods of liquid-state graph theory. Clearly these equations are matrix generalisations of the corresponding equations in I. For simplicity we now confine our attention to a two-level system, with levels 0 and 1: extension of the following analysis to a greater number of levels per site is trivial but cumbersome.

We begin by considering the locator series for the off-diagonal $G_{ij}^{\alpha\beta}(z)$, which results from expanding the inverse in equation (3b). The mth term in this series consists of all transfer matrix element products with m $V_{kl}^{\gamma\delta}$ bonds linking $s \leq m + 1$ sites. In what follows, $i = 1, 2, \ldots$ as the argument of a function is used as a shorthand for $\boldsymbol{R}_i$, and $\mathrm{d}(i) \equiv \mathrm{d}\boldsymbol{R}_i$. The averaged off-diagonal Green function, defined by (6b), may thus be written as

$$\bar{G}^{\alpha\beta}(12) = \sum_{s=2}^{\infty} \int \ldots \int \rho^{s-2} g_s(1, 2, \ldots, s) \mathcal{G}_s^{\alpha\beta}(1, 2, \ldots, s) \, \mathrm{d}(3) \ldots \mathrm{d}(s) \tag{7}$$

where $g_s(1, 2, \ldots, s)$ is the normalised s-body distribution function for particles interacting via Φ_N (see, e.g., Hansen and McDonald 1986). $\mathcal{G}_s^{\alpha\beta}(1, 2, \ldots, s)$ stands for

the sum of all terms contributing to the off-diagonal $G_{ij}^{\alpha\beta}$ which involve exactly s sites. Each term on the right-hand side of (7) can be represented in terms of composite graphs consisting of s points and five types of connectors. First, there will in general be connectors from the $g_s(1, 2, \ldots, s)$ factors which we will comment on later. Second, there is a continuous and directed chain composed of the four types of $V_{ij}^{\alpha\beta}$ bonds, namely V_{ij}^{00}, V_{ij}^{01}, V_{ij}^{10} and V_{ij}^{11}; in practice we will take $V_{ij}^{01} = V_{ij}^{10}$. The chain (which is continuous in both site and level indices) begins on level α of site 1, touches each of the s points at least once on either level 0 or level 1 or both, and ends on level β of site 2. We define a 0 stage (1 stage) as a contact of this V chain with level 0 (1) of a point. In traversing the chain, any point and any bond may occur any number of times, and all possible alternations of 0 and 1 stages at successive interior stages are allowed, an interior stage being any stage other than the end stage associated with level α of site 1 or the end stage associated with level β of site 2. A factor of z_γ^{-1} is associated with each γ stage. Thus $\mathcal{G}_s^{\alpha\beta}(1, 2, \ldots, s)$ is the sum of all chain continuous graphs connecting s sites, beginning on level α of site 1 and ending on level β of site 2, and having any number of 0 (1) interior stages; with each 0 (1) stage is associated a factor of $z_0^{-1}(z_1^{-1})$. The initial (1) and final (2) points of the graphs in $\bar{G}^{\alpha\beta}(12)$ are not integrated over and are root points (RP) in graph-theory terminology. All other points are integrated over and are field points (FP); with each FP is associated a factor of ρ.

The above specification of the graphs contributing to $\bar{G}^{\alpha\beta}(12)$ is a simple generalisation of that used in I for the graphs contributing to the one-level averaged Green function $\bar{G}(12)$, and it is straightforward to derive the graphs in $\bar{G}^{\alpha\beta}(12)$ from those in $\bar{G}(12)$: consider any graph in $\bar{G}(12)$ consisting of s points and m stages; for each such graph there will be 2^{m-2} graphs in $\bar{G}^{\alpha\beta}(12)$ with the same V-chain topology, reflecting the fact that each of the $m-2$ interior stages may be a 0 or a 1 stage. There is thus a $1:2^{m-2}$ correspondence between the graphs in $\bar{G}(12)$ and those in $\bar{G}^{\alpha\beta}(12)$. A similar generalisation for graphs contributing to the averaged diagonal Green function $\bar{G}^{\alpha\beta}(z)$ follows directly from equations (6*a*) and (7), which give

$$z_\alpha \bar{G}^{\alpha\beta}(z) = \delta_{\alpha\beta} + \sum_\gamma \sum_{s=2}^{\infty} \int \ldots \int \rho^{s-1} V^{\alpha\gamma}(12) \mathcal{G}_s^{\gamma\beta}(2, 1, \ldots, s) \times g_s(2, 1, \ldots, s)\, \mathrm{d}(2)\, \mathrm{d}(3) \ldots \mathrm{d}(s). \tag{8}$$

A topological analysis and renormalisation of the composite interaction graphs contributing to $\bar{G}^{\alpha\beta}(12)$ follows along lines similar to that given in I for the one-level $\bar{G}(12)$, to which the reader is referred for further details. We shall therefore merely summarise the relevant procedure. The graphs contributing to $\bar{G}^{\alpha\beta}(12)$ and $\bar{G}^{\alpha\beta}(z)$ are composite, and so both factors ($\mathcal{G}_s^{\alpha\beta}$ and g_s) in the integrands of equations (7) and (8) contribute to their topological properties. The degree of connectivity of a composite graph clearly exceeds or equals the degree of connectivity of the associated chain-continuous V-bond component stemming from $\mathcal{G}_s^{\alpha\beta}$. As in I, therefore, one examines first the case of a perfectly random system for which $g_s(1, 2, \ldots, s) = 1$ for all s, and considers the topology of the interaction graphs consisting solely of V chains which contribute to the resultant averaged Green functions (denoted in this limit by $\bar{G}_0^{\alpha\beta}(12)$ and $G_0^{\alpha\beta}(z)$). The analysis of I requires slight modification due to the presence of more than one level per site, but the essential topological reduction again consists of eliminating one-articulation points (1-AP), thereby renormalising the stages or vertices, together with a subsequent elimination of one-bridge points (1-BP). Having performed a topological reduction for the perfectly random system, one then considers the additional

connectors arising from the $g_s(1, 2, \ldots s)$ distribution functions which characterise the quenched liquid-like structure: this aspect of the problem is identical to that in I. The 1-AP and 1-BP of the composite interaction graphs contributing to the averaged Green functions are then eliminated, and the topological reduction is thus complete. We now summarise the essential results of this procedure.

From conventional liquid-state theory

$$g_s(1, 2, \ldots, s) = \prod_{t=2}^{s} \prod_{\text{all } Q_t} [1 + \gamma_t(Q_t)] \tag{9}$$

where Q_t stands for a particular combination of t of the points from $1, 2, \ldots,$ s. The direct connector $\gamma_t(1, 2, \ldots, t)$ is the sum of all terms connecting any pair of points in the set $(1, 2, \ldots, t)$ without going through another member of the set. Taking into account these spatially short-ranged γ connectors, a topological reduction of $\bar{G}^{\alpha\beta}(12)$ leads to the result

$$\bar{G}^{\alpha\beta}(12) = \sum_{\gamma,\delta} \bar{G}^{\alpha\gamma}(z) H^{\gamma\delta}(12) \bar{G}^{\delta\beta}(z) \tag{10a}$$

where

$$H^{\alpha\beta}(12) = C^{\alpha\beta}(12) + \rho \sum_{\gamma,\delta} \int \mathrm{d}(3) H^{\alpha\gamma}(13) \bar{G}^{\gamma\delta}(z) C^{\delta\beta}(32). \tag{10b}$$

Elimination of the 1-AP is reflected in equations (10) by the presence of averaged diagonal Green functions $\bar{G}^{\alpha\beta}(z)$ at each renormalised stage; and elimination of the 1-BP is reflected in (10*b*) where the irreducible unit $C^{\alpha\beta}(12)$ lacks 1-BP. Expressed in fully renormalised form (lacking 1-AP as well as 1-BP), the function $C^{\alpha\beta}(12)$ is said to be strongly irreducible and is specified as the sum of all composite graphs with two RP at the end stages (being labelled 1 and 2 and associated with factors of unity), a factor of ρ associated with each FP, no 1-BP, no 1-AP and an appropriate factor of $\bar{G}^{\gamma\delta}(z)$ associated with each interior stage. (Note in consequence that a $V^{01}(i, j)$ bond may be contiguous at FP j with, e.g., a $V^{00}(j, k)$ bond by virtue of a factor of $\bar{G}^{10}(z)$ being associated with a stage at FP j.) A given composite graph of s points in $C^{\alpha\beta}(12)$ consists of its corresponding chain graph component together with a factor from $g_s(1, 2, \ldots, s)$ with sufficient γ connectors to render the composite graph strongly irreducible. An algorithm to determine this factor is given in § 5 of Wertheim's (1973) paper, and we do not repeat it here. The graphs in each $C^{\alpha\beta}(12)$ can be generated simply from those in the one-level $C(12)$ (see figure 3 of I). For each graph containing m interior stages in the renormalised $C(12)$ there will be 4^m graphs in the renormalised $C^{\alpha\beta}(12)$ with the same V-chain topology, as follows from the fact that there are four possible decortions at each interior stage, namely any of the $\bar{G}^{\alpha\beta}(z)$. For a particular combination of decorations, the nature of the connecting V bonds is uniquely determined by α, β and the choice of decorations; and the associated factor from $g_s(1, 2, \ldots, s)$ is identical to that associated with the corresponding graph in $C(12)$. In figure 1 we give an example of a composite graph in the one-level $C(12)$, together with the corresponding graphs in $C^{01}(12)$, of which there are four since there is only one interior stage. Note that the graphs in $C^{01}(12)$ can also be generated from those in $C^{00}(12)$ simply by changing the last bond of the chain graph component from $V^{00}(j2)$ to $V^{01}(j2)$, or from $V^{10}(j2)$ to $V^{11}(j2)$, and similarly for $C^{10}(12)$ and $C^{11}(12)$.

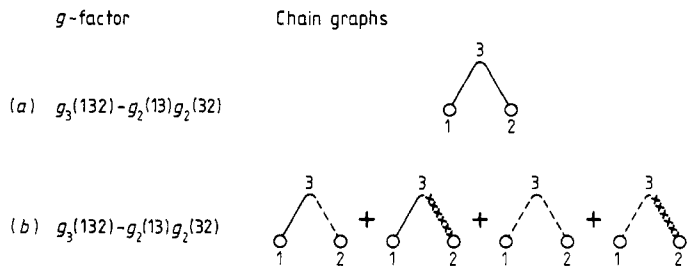

Figure 1. Example of (*a*) a composite, renormalised graph contributing to the one-level $C(12)$, together with (*b*) the corresponding graphs in $C^{01}(12)$. $\underset{i}{\circ}\!\!-\!\!-\!\!\underset{j}{\circ}$ denotes a V_{ij}^{00} bond, $\underset{i}{\circ}\!\!-\!\!-\!\!-\!\!-\!\!\underset{j}{\circ}$ a V_{ij}^{01} or V_{ij}^{10} bond, and $\underset{i}{\circ}\!\times\!\times\!\times\!\times\!\underset{j}{\circ}$ a V_{ij}^{11} bond. A factor of unity is associated with each RP, a factor of $\rho\bar{G}(z)$ with the FP in (*a*), and factors of $\rho\bar{G}^{00}(z)$, $\rho\bar{G}^{01}(z)$, $\rho\bar{G}^{10}(z)$ and $\rho\bar{G}^{11}(z)$ respectively with the FP of each graph in (*b*).

Finally, equations (10*a*) and (6*a*) may be combined to give the following exact self-consistency equation for the averaged diagonal Green functions:

$$z_\alpha \bar{G}^{\alpha\beta}(z) = \delta_{\alpha\beta} + \rho \sum_{\gamma,\delta,\varepsilon} \int \mathrm{d}(2) V^{\alpha\gamma}(12)\bar{G}^{\gamma\delta}(z)H^{\delta\varepsilon}(21)\bar{G}^{\varepsilon\beta}(z) \tag{11}$$

with $H^{\alpha\beta}(12)$ given from (10*b*).

3. Exact theory and some general features

To avoid a surfeit of superscripts it is convenient to adopt a matrix notation. Equations (10*b*) and (11) can be recast as

$$\mathbf{H}(12) = \mathbf{C}(12) + \rho \int \mathrm{d}(3)\mathbf{H}(13)\bar{\mathbf{G}}(z)\mathbf{C}(32) \tag{12}$$

$$\mathbf{z}\bar{\mathbf{G}}(z) = \mathbf{I} + \rho \int \mathrm{d}(2)\mathbf{V}(12)\bar{\mathbf{G}}(z)\mathbf{H}(21)\bar{\mathbf{G}}(z) \tag{13}$$

where $\mathbf{I}$ is the identical matrix, $(\mathbf{z})^{\alpha\beta} = z_\delta \delta_{\alpha\beta}$, and all other matrices are such that $(\mathbf{M})^{\alpha\beta} = M^{\alpha\beta}$. Defining the Fourier transform of any matrix function $\mathbf{M}(\boldsymbol{R})$ by

$$\hat{\mathbf{M}}(\boldsymbol{k}) = \int \mathrm{d}\boldsymbol{R} \exp(-\mathrm{i}\boldsymbol{k}\cdot\boldsymbol{R})\mathbf{M}(\boldsymbol{R})$$

and using translational invariance, equation (12) may be inverted to give

$$\hat{\mathbf{H}}(\boldsymbol{k}) = \hat{\mathbf{C}}(\boldsymbol{k})(\mathbf{I} - \rho\bar{\mathbf{G}}(z)\hat{\mathbf{C}}(\boldsymbol{k}))^{-1}. \tag{14}$$

Equation (13) thus reduces to

$$\mathbf{z}\bar{\mathbf{G}}(z) = \mathbf{I} + \rho \int \frac{\mathrm{d}\boldsymbol{k}}{(2\pi)^3} \hat{\mathbf{V}}(\boldsymbol{k})\bar{\mathbf{G}}(z)\hat{\mathbf{C}}(\boldsymbol{k})(\mathbf{I} - \rho\bar{\mathbf{G}}(z)\hat{\mathbf{C}}(\boldsymbol{k}))^{-1}\bar{\mathbf{G}}(z) \tag{15}$$

$$= \mathbf{I} + \mathbf{S}(z)\bar{\mathbf{G}}(z) \tag{16}$$

where the self-energy matrix $\mathbf{S}(z) \equiv \mathbf{S}(\bar{\mathbf{G}}(z))$ is thus defined and is such that $\bar{\mathbf{G}}(z) = (\mathbf{z} - \mathbf{S}(z))^{-1}$.

If $\hat{\mathbf{C}}(k)$ is known explicitly as a function of k and $\bar{\mathbf{G}}(z)$ then equation (15), which is a matrix generalisation of that derived in I, constitutes an exact self-consistency equation for the averaged diagonal Green functions, $\bar{G}^{\alpha\beta}(z)$. (Note also that although the above equations have been derived for a two-level system they apply equally to the general case of an n-level system, with the 2×2 matrix functions being replaced by $n \times n$ matrices.) As discussed in § 2 and also I, however, although we do have an algorithm for the construction of all graphs in $\mathbf{C}(12)$, we do not have exact closed expressions for these functions, and must therefore resort to approximation. All the approximations discussed in I and II can be generalised to a multi-level system, but in this paper we consider only three such. First we examine the so called Hubbard approximation which, although somewhat simplistic, brings out many of the features of more sophisticated theories. In the following sections we then discuss single-site theories, in particular the SSCA/EMA and the MTA, to which the former reduces in the limit of a perfectly random system. Before we consider specific approximations, however, we will examine the exact equations just derived, in one particular limit, that in which the transfer matrix elements are independent of the levels α and β: $V^{\alpha\beta}(12) \equiv V(12)$. With one possible exception (discussed below) this limit is unrealistic, but it illustrates clearly, and with minimum effort, two general features of the density of states of a two-level system.

Remember that all graphs in each $C^{\alpha\beta}(12)$ have a factor of unity associated with the end stages; the only difference between corresponding graphs in the different $C^{\alpha\beta}(12)$ functions lies in the nature of the first and last V bonds. But in the limit of all transfer matrix elements being identical, this difference disappears and the $C^{\alpha\beta}(12)$ functions all coincide; the same argument applies to $H^{\alpha\beta}(12)$. Thus, writing $H^{\alpha\beta}(12) \equiv H_{\mathrm{T}}(12)$ and $C^{\alpha\beta}(12) \equiv C_{\mathrm{T}}(12)$ for all α and β, equation (12) reduces to

$$H_{\mathrm{T}}(12) = C_{\mathrm{T}}(12) + \rho \bar{G}_{\mathrm{T}}(z) \int \mathrm{d}(3) H_{\mathrm{T}}(13) C_{\mathrm{T}}(32) \tag{17a}$$

where

$$\bar{G}_{\mathrm{T}}(z) = \bar{G}^{00}(z) + \bar{G}^{01}(z)\bar{G}^{10}(z) + \bar{G}^{11}(z). \tag{17b}$$

Similarly, equation (13) reduces to

$$\mathbf{z}\bar{\mathbf{G}}(z) = \mathbf{I} + S_{\mathrm{T}}(z)\mathbf{1}\bar{\mathbf{G}}(z) \tag{18a}$$

where $\mathbf{1}$ is a 2×2 matrix with all elements unity, and $S_{\mathrm{T}}(z)$ is given by

$$S_{\mathrm{T}}(z) = \rho \bar{G}_{\mathrm{T}}(z) \int \mathrm{d}(2) V(12) H_{\mathrm{T}}(21). \tag{18b}$$

Rearranging (18a) gives

$$\begin{bmatrix} \bar{G}^{00}(z) & \bar{G}^{01}(z) \\ \bar{G}^{10}(z) & \bar{G}^{11}(z) \end{bmatrix} = [z_0 z_1 - (z_0 + z_1) S_{\mathrm{T}}(z)]^{-1} \begin{bmatrix} z_1 - S_{\mathrm{T}}(z) & S_{\mathrm{T}}(z) \\ S_{\mathrm{T}}(z) & z_0 - S_{\mathrm{T}}(z) \end{bmatrix} \tag{19}$$

and summing all elements of the matrices together yields

$$\bar{G}_{\mathrm{T}}(z) = (A(z) - S_{\mathrm{T}}(z))^{-1} \tag{20a}$$

where

$$A(z) = z_0 z_1 / (z_0 + z_1). \tag{20b}$$

Equations (17), and equations (20) and (18b), are mathematically equivalent to the one-level results derived in I, with $\bar{G}_{\mathrm{T}}(z)$ replacing the one-level $\bar{G}(z)$ and $A(z)$ replacing the energy z.

With one important exception that we discuss shortly, two general results follow from these equations. First, for all possible values of the physical parameters (such as the number density, ρ, of sites), there is always a band gap in the total density of states $D_0(E) + D_1(E)$, lying between the zero-order site energies ε_0 and $\varepsilon_1 > \varepsilon_0$. This can be seen by considering the energy $z = (\varepsilon_0 + \varepsilon_1)/2 + i\eta$. In the limit that $\eta \to 0+$, $z_0 + z_1$ vanishes and consequently $A(z)$ diverges. Thus from equations (20*a*) and (18*b*) we see that $\bar{G}_T(z)$ and $S_T(z)$ vanish, and equation (19) reduces to $\bar{\mathbf{G}}(z) = \mathbf{z}^{-1}$. Hence, for some energy interval between ε_0 and ε_1, $\bar{\mathbf{G}}(z)$ is real and the DOS must be zero; the existence and persistence of this band gap for the case of identical $V^{\alpha\beta}(12)$ has also been seen in computer simulations of the model system (Bush *et al* 1989b). For a more realistic set of non-coincident $V^{\alpha\beta}(12)$ we will show later that, although the two bands centred about ε_0 and ε_1 can overlap, they often do so less readily than one might expect due to a significant repulsion between the bands. A simple physical explanation can be given for this effect. Roughly speaking, the broadening of the uncoupled 0 and 1 bands is proportional to $V^{00}(12)$ and $V^{11}(12)$ respectively. The bands are, however, coupled via the $V^{01}(12)$ interaction, and this coupling produces a repulsion between the bands approximately proportional to $V^{01}(12)$. When $V^{00}(12)$ and $V^{11}(12)$ exceed $V^{01}(12)$ the broadening overcomes the repulsion and the two bands can merge; but in the converse case the repulsion dominates and there is a band gap between the two sub-bands. The case of identical $V^{\alpha\beta}(12)$ represents a crossover point at which the broadening effects just fail to overcome the repulsion.

In passing we would add that Hubbard's (1963) original treatment of electron correlation effects in narrow energy bands effectively mapped that problem onto a two-level, one-electron, tight-binding model with identical $V^{\alpha\beta}(12)$: with the replacements $(E - \varepsilon_0)^{-1} \to (1 - n_{-\sigma})(E - T_0)^{-1}$ and $(E - \varepsilon_1)^{-1} \to n_{-\sigma}(E - T_0 - I)^{-1}$ (where I is the on-site 'Hubbard U'), and identifying Hubbard's $G_{ij}^{\sigma}(E)$ with $\Sigma_{\alpha,\beta}\, G_{ij}^{\alpha\beta}(E)$, Hubbard's (1963) equation (51) (or (18) of Hubbard (1964)) reduces to our equation (3*a*) for the case $V_{ij}^{\alpha\beta} \equiv V_{ij}$. Hubbard indeed found that the two sub-bands of the pseudoparticle spectrum failed to overlap. This feature is a direct consequence of the approximate mapping described above, is physically unsound in the context of the correlation problem, and was alleviated in Hubbard's (1964) improved solution of the correlation problem.

The second general feature of equations (17)–(20) above concerns band mixing, i.e. the contribution of 1-level states to the band centred about ε_0, and *vice versa*. From equation (19) we see that if $z = \varepsilon_0 + i\eta$, then as $\eta \to 0+$, z_0 vanishes and $\bar{G}^{11}(z) \to 1/z_1$; thus $D_1(\varepsilon_0) = 0$, and similarly $D_0(\varepsilon_1) = 0$. It can, however, be easily shown that, for all other energies, if $D_0(E) \neq 0$ then Im $S_T(E) \neq 0$ and consequently $D_1(E) \neq 0$, i.e. there is mixing throughout the sub-bands except at the energies $E = \varepsilon_0$ and $E = \varepsilon_1$. Again this general pattern carries over to the case of a more realistic set of (non-coincident) $V^{\alpha\beta}(12)$, with (usually) $D_0(\varepsilon_1) = 0$, $D_1(\varepsilon_0) = 0$, and mixing throughout the rest of the bands.

The aforementioned exception to the identical $V^{\alpha\beta}(12)$ results described above occurs in the degenerate case where $\varepsilon_0 = \varepsilon_1$. In this case, at the energy $z = (\varepsilon_0 + \varepsilon_1)/2 + i\eta$, $z_0 = z_1 = i\eta$ and in the limit $\eta \to 0+$, $A(z)$, instead of diverging, tends to zero. As a result it can be shown that, at this energy, $\bar{G}_T(z)$ and $\bar{S}_T(z)$ are non-vanishing pure imaginary quantities. Further, it follows from equation (19) that $D_0(E) = D_1(E)$ for all E, and neither DOS vanishes at the energy $\varepsilon_0 = \varepsilon_1 \equiv \frac{1}{2}(\varepsilon_0 + \varepsilon_1)$. Therefore, the above two general features are no longer valid and instead there are two identical bands arising from the doubly degenerate level at energy $\varepsilon_0 = \varepsilon_1$. We can extend this trivially to n levels divided between m degenerate sets, in which case the problem reduces to an

m-level problem, each level giving rise to the appropriate number of identical bands. This suggests a means of dealing with sets of p, d and f orbitals, although it must be remembered that in these cases symmetry conditions are important and consequently the transfer matrix elements within a given set of such orbitals will not in general be identical (see, e.g., Yonezawa and Martino 1976).

We now turn to the first and simplest of the approximate theories for the DOS considered in this paper. As shown in I, the familiar one-level Hubbard semi-elliptic DOS arises from the two approximations $H(12) \simeq C(12)$ and $C(12) \simeq V(12)g_2(12)$ to the one-level functions, where $g_2(12)$ is the pair distribution function. We expect this approximation to be qualitatively reasonable at low densities (although, as discussed in I, it does not reproduce correctly the exact $\rho \to 0$ limit). The obvious generalisation to a multi-level system is to approximate (12) by $\mathbf{H}(12) \simeq \mathbf{V}(12)g_2(12)$, in which case the self-energy matrix reduces to

$$\mathbf{S}(z) \simeq \rho \int \mathrm{d}(2) g_2(12)\mathbf{V}(12)\bar{\mathbf{G}}(z)\mathbf{V}(21). \tag{21}$$

With a specified pair distribution function and set of transfer matrix elements, $\bar{\mathbf{G}}(z)$ can be found via a simple iteration of equations (16) and (21); equation (5b) then gives the averaged DOS arising from each level.

For all three of the approximate theories considered in this paper, we choose a set of Yukawa transfer matrix elements:

$$V^{\alpha\beta}(R) = (-V_0 a^{\alpha\beta}/R)\exp(-\alpha^{\alpha\beta}R). \tag{22}$$

Here we take each $V^{\alpha\beta}(12)$ to be a function solely of $R = |\boldsymbol{R}_1 - \boldsymbol{R}_2|$, i.e. we assume spherical symmetry, a case strictly appropriate to s orbitals. A modified exponential transfer matrix element is known to be appropriate to several problems of physical interest, such as electronic transport in tightly bound bands of certain liquid metals and alloys, the impurity band of some doped semiconductors, and triplet electronic excitons in the impurity band of isotopically mixed organic solids; the specific choice of a Yukawa form is for the sake of simplicity. It should be noted that the sign of $V^{01}(R)$ is irrelevant, because the DOS depends on $\bar{G}^{00}(z)$ and $\bar{G}^{11}(z)$, the constituent graphs of which must always contain an even number of V_{ij}^{01} bonds. However the signs of $V^{\alpha\alpha}(R)$ do matter, and physical arguments suggest that both $V_0 a^{00}$ and $V_0 a^{11}$ should be positive. Although equations (16) and (21) are readily solved for any input $g_2(R)$, for the sake of later comparison with the SSCA/EMA results we here consider a simple step function $g_2(R)$, corresponding to the low-density limit of a hard-sphere fluid with hard-sphere diameter, σ: i.e.

$$g_2(R) = \theta(R - \sigma) \tag{23}$$

where θ is the unit step function.

With these choices of $V^{\alpha\beta}(R)$ and $g_2(R)$, the integration in (21) is trivial, yielding $\mathbf{S}(z)$ as a simple function of the $\bar{G}^{\alpha\beta}(z)$. Here it is convenient to define a set of reduced (dimensionless) variables. If we choose σ as the unit of length and $V_0^* = V_0/\sigma$ as the unit of energy (so that the $a^{\alpha\beta}$ are dimensionless), then we may define the reduced parameters

$$\rho^* = \rho\sigma^3 \qquad \tilde{\alpha}^{\alpha\beta} = \alpha^{\alpha\beta}\sigma \qquad \tilde{z} = z/V_0^* \tag{24a}$$

and also the reduced functions

$$\tilde{\mathbf{S}}(z) = \mathbf{S}(z)/V_0^* \qquad \tilde{\mathbf{G}}(z) = V_0^* \bar{\mathbf{G}}(z). \tag{24b}$$

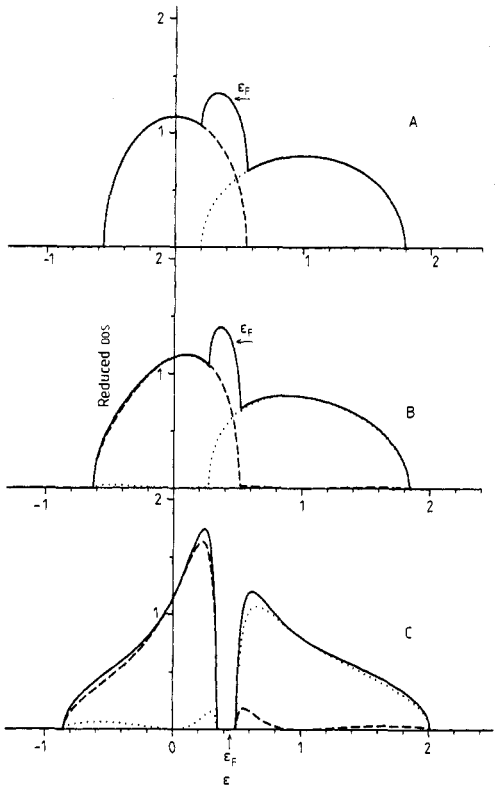

Figure 2. $\tilde{D}_0(\varepsilon)$ (broken curve), $\tilde{D}_1(\varepsilon)$ (dotted curve) and $\tilde{D}_0(\varepsilon) + \tilde{D}_1(\varepsilon)$ (full curve) in the Hubbard model for $\rho^* = 0.1$, $\Delta\varepsilon = 1$, all $\tilde{\alpha}^{\alpha\beta} = 0.8$, $a^{00} = 0.7$, $a^{11} = 1$ and (A) $a^{01} = 0$, (B) $a^{01} = 0.3$, and (C) $a^{01} = 0.7$.

The reduced DOS from level α is then given by

$$\tilde{D}_\alpha(\varepsilon) = V_0^* D_\alpha(\varepsilon) = -\pi^{-1} \operatorname{Im}[G^{\alpha\alpha}(\varepsilon + i\eta)] \tag{25}$$

where we decompose the reduced energy as $\tilde{z} = \varepsilon + i\eta$ ($\eta \to 0+$). The system has one other parameter, namely the reduced separation of the zero-order energies, $\Delta\varepsilon = (\varepsilon_1 - \varepsilon_0)/V_0^*$. We will set the zero of the energy scale at ε_0 so that the zero-order 1 level is at a reduced energy $\varepsilon = \Delta\varepsilon$.

In figures 2–4 we plot the resultant reduced DOS from level 0 ($\tilde{D}_0(\varepsilon)$, broken curve), from level 1 ($\tilde{D}_1(\varepsilon)$, dotted curve) and the total reduced DOS ($\tilde{D}_0(\varepsilon) + \tilde{D}_1(\varepsilon)$, full curve) for a variety of parameters. In figure 2 we consider a fixed density $\rho^* = 0.1$, $\Delta\varepsilon = 1$, all $\tilde{\alpha}^{\alpha\beta} = 0.8$, $a^{00} = 0.7$ and $a^{11} = 1$, and we investigate the effect of band coupling by taking three different values of a^{01} ($= a^{10}$), namely $a^{01} = 0$ (spectrum A), $a^{01} = 0.3$ (spectrum B) and $a^{01} = 0.7$ (spectrum C). Spectrum A is the case of two uncoupled bands, each having the familiar semi-elliptic shape characteristic of the Hubbard approximation for a one-level system; note that the upper band is broader as $a^{11} > a^{00}$. From B and C we see that one effect of a non-zero a^{01} is to make each band asymmetric, in contrast to uncoupled bands which are always symmetric about the appropriate zero-order site energy. Also, as expected, the degree of mixing between the bands increases with a^{01}. More specifically, for $a^{01} \neq 0$ there is mixing throughout the bands except at the zero-order energies ε_0 and ε_1, as found previously for the limiting case of identical transfer matrix elements. The most pronounced feature is, however, the appearance of a band

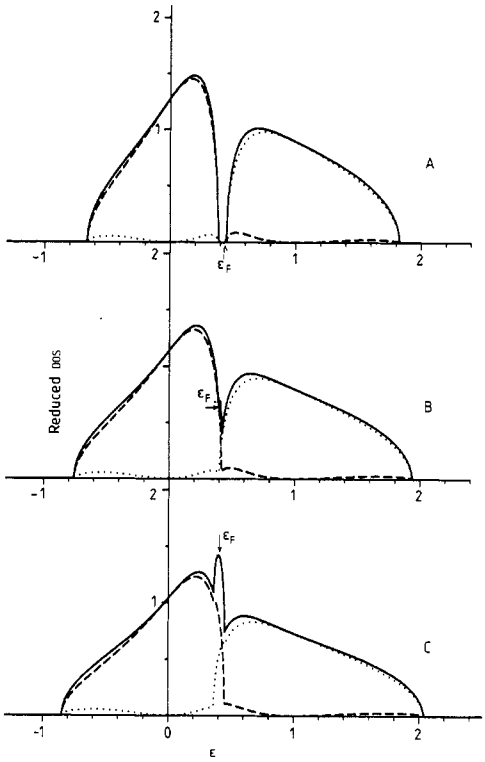

Figure 3. As figure 2 but with a fixed $a^{01} = 0.55$ and (A) $\rho^* = 0.08$, (B) $\rho^* = 0.1$ and (C) $\rho^* = 0.12$.

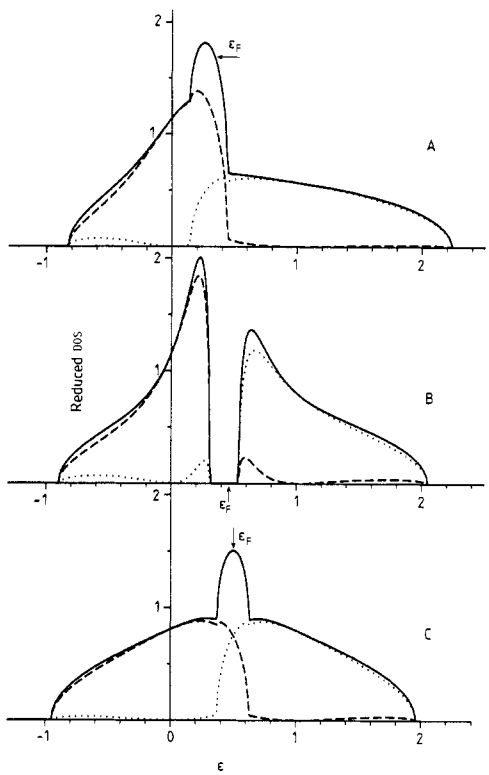

Figure 4. As figure 2 but with a fixed $a^{01} = 0.55$ and (A) $\tilde{\alpha}^{11} = 0.6$, (B) $\tilde{\alpha}^{01} = 0.6$ and (C) $\tilde{\alpha}^{00} = 0.6$.

gap in spectrum C of figure 2, which again arises because interlevel coupling, embodied in a^{01}, produces a repulsion between the sub-bands and eventually a band gap. (Note that a^{01} is significantly smaller than a^{11} here: the existence of a gap is not dependent upon identical $V_{ij}^{\alpha\beta}$.) The repulsion also manifests itself in the bottom (top) of the lower (upper) band moving outwards, such that the widths of the sub-bands in spectrum C are similar to those of the uncoupled bands (spectrum A). Finally, although spectrum B shows the above features, it is still rather similar to spectrum A, showing that, with the chosen ρ^*, $\Delta\varepsilon$, $\tilde{\alpha}^{\alpha\beta}$ and $a^{\alpha\alpha}$, there must be appreciable interlevel coupling before major qualitative changes occur in the total DOS.

Numerical integration shows that all the spectra in figures 2–4 are correctly normalised to two. We can thus determine accurately the Fermi energy, ε_F, defined (at $T = 0$) by

$$\int_{\varepsilon_-}^{\varepsilon_F} (\tilde{D}_0(\varepsilon) + \tilde{D}_1(\varepsilon))\, \mathrm{d}\varepsilon = \tfrac{1}{2}n \tag{26}$$

where ε_- is the lowest spectral band edge and n is the mean number of electrons per atom. Two cases are of particular interest. First, if $n = 1$ and there is no interlevel coupling, then the lower band will be half full and the upper band empty; by adding a non-zero a^{01} we may investigate the effect of an excited level on a half-filled valence

band (and within a one-electron description). For all three spectra shown in figure 2 we find in fact that the $n = 1$ Fermi energy is constant at $\varepsilon_F = 0$, and the total DOS at ε_F is approximately constant. Because of this, and since $\tilde{D}_1(0) = 0$, it appears that at the Hubbard level of description and for $n = 1$, the excited level will have little effect on properties associated with Fermi energy electrons, such as the conductivity in a delocalised regime.

The second case of particular interest is $n = 2$, corresponding to a full valence band interacting with an (initially) empty conduction band, a case important generally for metal–insulator transitions occurring in, e.g., divalent materials such as Hg or the alkaline earths, or for the rare gases; ε_F for the $n = 2$ case is marked in figures 2–4. Whenever there is a band gap we find that each sub-band is separately normalised to unity; consequently ε_F lies in the gap and the system is an insulator. As the band gap disappears, the DOS at ε_F becomes non-zero, at which point we would have a Wilson band-crossing insulator–metal transition were it not for the effects of disorder, which initially lead to states at ε_F being Anderson localised. An insulator–metal transition then occurs when states at ε_F in the pseudogap become delocalised. From figure 2 we see that band crossing, with the subsequent formation of a pseudogap, may be brought about by the diminution of a^{01}, but it is more natural to regard the formation and evolution of a pseudogap as being consequent upon an increase in density.

In figure 3, therefore, we take $\Delta\varepsilon = 1$, all $\tilde{\alpha}^{\alpha\beta} = 0.8$, $a^{00} = 0.7$, $a^{01} = 0.55$ and $a^{11} = 1$, and we progressively increase ρ^* from 0.08 (spectrum A) through 0.1 (B) to $\rho^* = 0.12$ (spectrum C); spectrum B has the same parameters as those in figure 2, apart from a different a^{01} chosen so that the band gap disappears for ρ^* slightly less than 0.1. For $\rho^* = 0.08$ there is a gap between the two sub-bands, in which ε_F lies for $n = 2$, the system being an insulator. As ρ^* increases towards 0.1 (spectrum B) the two bands overlap forming a narrow, deep pseudogap in which lies ε_F. Since $\tilde{D}(\varepsilon_F)$ is small, it is likely that states at the Fermi energy are Anderson localised, the system retaining its insulating behaviour. We would, however, add that while a knowledge of the DOS is an ingredient in a theory of localisation—which is one motivation for this work—it is not by itself sufficient to determine whether states in the pseudogap are localised or extended. Finally, as ρ^* increases towards 0.12 (spectrum C) the two sub-bands broaden further and the pseudogap all but disappears; note further that in spectrum C the bands have broadened sufficiently to give a maximum in the total DOS at ε_F, which no longer lies in the remnant pseudogap. Two additional features in figure 3 should be noted. First, the pseudogap persists over a very narrow density range ($0.09 \leqslant \rho^* \leqslant 0.11$). This arises from the steep band edges inherent in the Hubbard level of approximation; we shall see later that single-site theories predict a more prolonged pseudogap. Second, and in contrast to the $n = 1$ case discussed above, it is evident from spectra B and C in figure 3 that $\tilde{D}_0(\varepsilon)$ that $\tilde{D}_1(\varepsilon)$ are comparable at ε_F for $n = 2$: the excited level will, for obvious physical reasons, have an appreciable effect on properties associated with Fermi energy electrons.

Finally, in figure 4 we take $\rho^* = 0.1$, $\Delta\varepsilon = 1$, $a^{00} = 0.7$, $a^{01} = 0.55$, $a^{11} = 1$, and we decrease in turn each of the $\tilde{\alpha}^{\alpha\beta}$ from the value of 0.8 used in figures 2 and 3 to a value of 0.6. By diminishing $\tilde{\alpha}^{\alpha\beta}$ we make the corresponding $V^{\alpha\beta}(R)$ longer ranged; we would expect this to have a similar qualitative effect to an increase in $a^{\alpha\beta}$. Thus, spectrum A in figure 4 differs from B in figure 3 only in having $\tilde{\alpha}^{11} = 0.6$, which we see broadens the upper band sufficiently to eliminate the pseudogap and produce a maximum in the DOS at ε_F. Similarly, spectrum B differs only in having $\tilde{\alpha}^{01} = 0.6$, producing a band gap by virtue of the longer-ranged $V^{01}(R)$, and spectrum C has $\tilde{\alpha}^{00} = 0.6$, thus broadening the

lower band sufficiently to produce a maximum in the DOS at ε_F for $n = 2$. Note that spectrum C is symmetric about $\varepsilon = 0.5$, despite the fact that $V^{00}(R)$ differs from $V^{11}(R)$. This arises because the Hubbard self-energy (equation (21)) depends on the second moments:

$$J_2^{\alpha\beta\gamma\delta} = \rho \int \mathrm{d}(2) V^{\alpha\beta}(12) V^{\gamma\delta}(21)\, g_2(12).$$

The parameters in spectrum C of figure 4 are such that $J_2^{0000} = J_2^{1111}$, although $J_2^{0001} \neq J_2^{1101}$ and so it appears that these cross moments are less significant. This suggests that a study of the variation in the range parameters $\tilde{\alpha}^{\alpha\beta}$ is to some extent superfluous, in that variation in the second moments can be adequately achieved via the strength parameters $a^{\alpha\beta}$.

4. Single-site theories

As in I we may specify an 'exact' single-site theory by two simple conditions:

(i) The $s \geqslant 3$-body structural correlation functions $g_s(1, 2, \ldots, s)$ are approximated by the Kirkwood superposition approximation.

(ii) Only single-site graphs are retained in $\mathbf{C}(12)$, meaning those renormalised graphs (free of 1-AP) in which only a single stage (which may be a 0 or a 1 stage) is associated with any point.

The familiar Kirkwood superposition approximation amounts to retaining only the $t = 2$ direct connector, $\gamma_2(12) = h_2(12)$ $(= g_2(12) - 1)$ in equation (9), which is thus decomposed approximately as

$$g_s(1, 2, \ldots, s) = \prod_{i=1}^{s-1} \prod_{j=i+1}^{s} (h_2(i, j) + 1). \tag{27}$$

Note that equation (12) (and thus equation (15)) is maintained, and the approximation is made directly to $\mathbf{C}(12)$; we denote the single-site approximation to $\mathbf{C}(12)$ by $\mathbf{C}_s(12)$. The graphs in each $C_s^{\alpha\beta}(12)$ may be generated from those in the one-level $C_s(12)$ (see figure 4 of I) in precisely the same way as graphs in the exact $C^{\alpha\beta}(12)$ are generated from the corresponding one-level graphs, as discussed in § 2. A single-site theory leads to a better description of the DOS at higher number densities, since at lower densities multiple hopping between pairs of sites will be important, and such processes are omitted in any single-site theory.

In practice, to produce a computationally tractable theory we must, as in I, make further approximations to the 'exact' single-site prescription. Many such approximations exist for the one-level case (see, e.g., Matsubara and Toyozawa 1961, Ishida and Yonezawa 1973, Roth 1974, 1976, Movaghar and Miller 1975), all of which can in principle be extended to the multi-level case (see, e.g., Yonezawa and Martino 1976, Yonezawa *et al* 1977, Figueira *et al* 1984). We will, however, concern ourselves with approximations that are topologically proper, meaning those that preserve equation (12) (and, consequently, (15)) and make approximations directly to the strongly irreducible unit $\mathbf{C}_s(12)$. Two such theories are the MTA and the SSCA/EMA. The MTA is the simpler, corresponding to a perfectly random system in which the effects of liquid-like structure are neglected by setting $g_s(1, 2, \ldots, s) = 1$ for all s. In this limit, all graphs in

$C_s^{\alpha\beta}(12)$ except the first become zero, and hence $\mathbf{C}_s(12) = \mathbf{V}(12)$. As described in II, the SSCA/EMA involves neglecting all graphs in $C_s^{\alpha\beta}(12)$ in which the interior $h_2(i,j)$ bonds (arising from (27)) cross. This leads to the relation

$$g_2(12)\mathbf{C}_s(12) = g_2(12)\mathbf{V}(12) + h_2(12)\mathbf{H}_s(12) \tag{28}$$

where $\mathbf{H}_s(12)$ is related to $\mathbf{C}_s(12)$ via equation (12). Equation (28), which is the basic approximation in the SSCA/EMA, provides a closure relation to equation (12), and these equations may be solved by exploiting analogies in conventional liquid-state theory, as we describe in the following section. In the limit of a perfectly random system, $g_2(12) = 1$, and equation (28) reduces to the MTA result which we now consider in more detail. With $\mathbf{C}_s(12) = \mathbf{V}(12)$, the MTA self-energy is given by

$$\mathbf{S}(z) = \rho \int \frac{\mathrm{d}\boldsymbol{k}}{(2\pi)^3} \hat{\mathbf{V}}(\boldsymbol{k})\bar{\mathbf{G}}(z)\hat{\mathbf{V}}(\boldsymbol{k})(\mathbf{I} - \rho\bar{\mathbf{G}}(z)\hat{\mathbf{V}}(\boldsymbol{k}))^{-1}. \tag{29}$$

For 2×2 matrices we have the identity

$$(\det(\mathbf{M}+\mathbf{N}))(\mathbf{M}+\mathbf{N})^{-1} \equiv (\det \mathbf{M})\mathbf{M}^{-1} + (\det \mathbf{N})\mathbf{N}^{-1} \tag{30}$$

where det denotes determinant. Hence equation (29) can be rewritten as

$$\mathbf{S}(z) = \rho \int \frac{\mathrm{d}\boldsymbol{k}}{(2\pi)^3} \frac{\hat{\mathbf{V}}(\boldsymbol{k})}{\det(\mathbf{I} - \rho\bar{\mathbf{G}}(z)\hat{\mathbf{V}}(\boldsymbol{k}))} [\bar{\mathbf{G}}(z)\hat{\mathbf{V}}(\boldsymbol{k}) - \rho \det(\hat{\mathbf{V}}(\boldsymbol{k}))\det(\bar{\mathbf{G}}(z))]. \tag{31}$$

With a specified set of transfer matrix elements, (31) can be evaluated to yield $\mathbf{S}(z)$ as a function of the $\bar{G}^{\alpha\beta}(z)$. Equation (16) gives $\bar{\mathbf{G}}(z)$ as a function of $\mathbf{S}(z)$, and a simple iteration of these two equations is sufficient to determine $\bar{\mathbf{G}}(z)$ and hence the DOS.

Here we study the Yukawa transfer matrix elements of equation (22), which have the Fourier transform

$$\hat{V}^{\alpha\beta}(\boldsymbol{k}) = \frac{-4\pi V_0 a^{\alpha\beta}}{(\alpha^{\alpha\beta})^2 + k^2} \tag{32}$$

where $k = |\boldsymbol{k}|$. Equation (31) is considerably simplified by assuming that the $V^{\alpha\beta}(R)$ all have the same R dependence (i.e., that $\alpha^{\gamma\delta} = \alpha$ for any γ, δ), although the relative magnitudes may still differ through the $a^{\alpha\beta}$. Some justification for this may be found in the Hubbard DOS studied in § 3, where we found that variation of the $a^{\alpha\beta}$ alone gave sufficient flexibility in the choice of transfer matrix elements. The sole length scale in the problem is now the 'effective Bohr radius', $a_H = \alpha^{-1}$, which, together with $V_0' = V_0\alpha$ (which has dimensions of energy) may be used to define the reduced parameters

$$\rho' = \rho\alpha^{-3} \qquad z' = z/V_0' \tag{33a}$$

and the reduced functions

$$\mathbf{S}'(z) = \mathbf{S}(z)/V_0' \qquad \bar{\mathbf{G}}'(z) = V_0'\bar{\mathbf{G}}(z). \tag{33b}$$

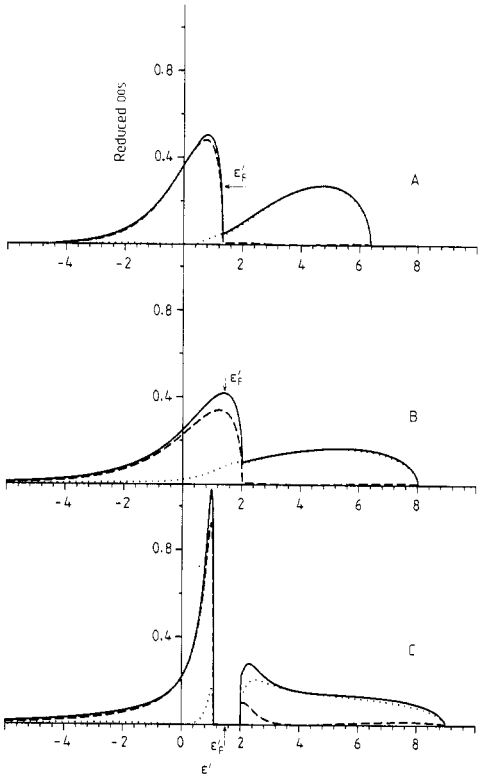

Figure 5. $D'_0(\varepsilon')$ (broken curve), $D'_1(\varepsilon')$ (dotted curve) and $D'_0(\varepsilon') + D'_1(\varepsilon')$ (full curve) in the MTA for $\Delta\varepsilon' = 4$, $a^{00} = 0.7$, $a^{11} = 1$ and (A) $\rho' = 0.3$, $a^{01} = 0.45$, (B) $\rho' = 1$, $a^{01} = 0.45$, and (C) $\rho' = 1$, $a^{01} = 0.85$. Note the different set of units used from those used in figures 2–4 and 6–8.

Equation (31) reduces to

$$\mathbf{S}'(z) = 8\rho' \left(\int_0^\infty \mathrm{d}k' \frac{k'^2}{(k'^2 + \mu)(k'^2 + \nu)} \right) \mathbf{a}\bar{\mathbf{G}}'(z)\mathbf{a}$$
$$+ 32\pi\rho'^2 \det(\mathbf{a}\bar{\mathbf{G}}'(z)) \left(\int_0^\infty \mathrm{d}k' \frac{k'^2}{(k'^2+1)(k'^2+\mu)(k'^2+\nu)} \right) \mathbf{a} \qquad (34a)$$

where $k' = k\alpha^{-1}$ and $-\mu$ and $-\nu$ are the solutions of

$$\det[(k'^2 + 1)\mathbf{I} + 4\pi\rho'\bar{\mathbf{G}}'(z)\mathbf{a}] = 0. \qquad (34b)$$

Evaluating the integrals gives

$$\mathbf{S}'(z) = \frac{4\pi\rho'}{\mu^{1/2} + \nu^{1/2}} \left[\mathbf{a}\bar{\mathbf{G}}'(z)\mathbf{a} + \left(\frac{4\pi\rho' \det(\mathbf{a}\bar{\mathbf{G}}'(z))}{(1+\mu^{1/2})(1+\nu^{1/2})} \right) \mathbf{a} \right]. \qquad (35)$$

Finally, equation (16) can be rewritten in reduced form as

$$\bar{\mathbf{G}}'(z) = (\mathbf{z}' - \mathbf{S}'(z))^{-1} \qquad (36)$$

where the non-zero elements of $\mathbf{z}'$ are $(\mathbf{z}')^{00} = z'$ and $(\mathbf{z}')^{11} = z' - \Delta\varepsilon'$. Iteration of equations (35) and (36) yields $\bar{\mathbf{G}}'(z')$ and hence the reduced DOS from level α given by

$$D'_\alpha(\varepsilon') \equiv V'_0 D_\alpha(\varepsilon') = -\pi^{-1} \operatorname{Im}[\bar{G}'^{\alpha\alpha}(\varepsilon' + \mathrm{i}\eta)] \qquad (37)$$

where we decompose the reduced energy as $z' = \varepsilon' + \mathrm{i}\eta$ ($\eta \to 0+$).

In figure 5 we plot $D'_0(\varepsilon')$ (broken curve), $D'_1(\varepsilon')$ (dotted curve) and the full DOS $D'_0(\varepsilon') + D'_1(\varepsilon')$ (full curve) for $\Delta\varepsilon' = 4$, $\rho' = 0.3$ (spectrum A) or $\rho' = 1$ (spectra B

and C), $a^{00} = 0.7$, $a^{01} = 0.45$ (A and B) or $a^{01} = 0.85$ (C), and $a^{11} = 1$. These spectra have similar qualitative features to those observed at the Hubbard level of approximation, although note the different reduced units used in the two theories. We will give later a direct comparison of the MTA and SSCA theories, but at present comparison between the MTA and Hubbard theories will be qualitative.

In spectra A and B of figure 5 we find that, although the coupling implied by a^{01} is not insignificant, D_0' and D_1' differ little from the corresponding uncoupled bands. This was also true of a moderate a^{01} in the Hubbard theory (see spectrum B, figure 2), but unlike the latter the uncoupled MTA DOS has a pronounced asymmetry with a long, low-energy tail. The principal effect in going from spectrum A to B is thus simply a broadening of the bands due to increasing ρ'. In going from spectrum B to C, however, we increase a^{01} to a value comparable to a^{00} and a^{11}, and this does lead to qualitative changes. As with the Hubbard approximation, the repulsion due to a^{01} produces a band gap and causes the outer band edges to move further outwards. Moreover, the asymmetry of the upper band is now reversed, so that the MTA DOS becomes qualitatively closer to that of the Hubbard DOS. In spectra A and C we have the usual pattern of mixing throughout the bands except at the zero-order energies. In spectrum B, however, we see that $D_1'(0)$ is non-zero. This is understandable since the coupling is relatively small and $D_1'(0)$ for the uncoupled bands is appreciable at $\rho' = 1$, but it is a useful reminder that there are exceptions to the usual pattern of mixing.

Numerical integration confirms that the MTA spectra are correctly normalised to two, and thus we may determine the Fermi energy, ε_F', defined via equation (26). For $n = 1$ and a single 0 band, the asymmetry characteristic of the MTA $D_0'(\varepsilon')$ means that ε_F' is blue shifted slightly to positive energies. Addition of an uncoupled excited level may lower ε_F' due to states in the low-energy tail of the excited band, but introduction of interlevel coupling produces in general two competing effects. First, the repulsion due to a non-zero a^{01} tends to push the 0 band to lower energies: this acts to decrease ε_F'. Second, the 1 band moves to higher energies, its low-energy tail is shortened considerably, and so states are effectively removed from the lower band; this tends to increase ε_F'. In going from spectrum B to C in figure 5 we find the second effect to be dominant so that ε_F', and consequently the total DOS at ε_F', increases. Further, for relatively weak a^{01}, $D_1'(\varepsilon_F')$ may be appreciable (see spectrum B). It appears therefore that at the MTA level of description, and in contrast to the Hubbard approximation, an excited level may have an appreciable effect on the nature of the Fermi level states of a half-filled valence band.

We now consider $n = 2$, for which ε_F' is marked in figure 5. As for the Hubbard DOS, whenever a band gap exists ε_F' lies in the gap and we have an insulator at $T = 0$. The gap may be created by decreasing ρ' or by increasing a^{01}, an example of the latter being given in spectrum C (the gap first appearing at $a^{01} = 0.8$). Just before the gap opens up there will be a pseudogap, such as that evident in spectrum A. On increasing ρ' the pseudogap becomes less pronounced, but it is still appreciable at $\rho' = 1$ (spectrum B). Although the pseudogap persists over a large density range, however, it is primarily the position of ε_F' and the character of Fermi level states which dictate the electrical properties of the system; and in spectrum B ε_F' is in fact close to the maximum in the total DOS, where the states are likely to be extended giving rise to a metallic state. As ρ' is decreased, ε_F' moves towards the pseudogap, but even in spectrum A the total DOS at ε_F' is relatively large. It is therefore possible that states at ε_F' are Anderson localised over a relatively small density range, although this can only be ascertained with confidence once a theory of localisation for a multi-level system has been developed.

5. The SSCA/EMA

In this section we consider in detail the SSCA/EMA which, as judged by computer simulations on the one-level problem (Bush *et al* 1989a), is likely to be the most successful approximate single-site theory for the DOS.

We need to solve equation (12) for the single-site $\mathbf{H}_s(12)$ and $\mathbf{C}_s(12)$, with the appropriate closure condition (28), to yield $\mathbf{H}_s(12)$ as a function of $\bar{\mathbf{G}}(z)$. Equation (13) (with $\mathbf{H}$ replaced by $\mathbf{H}_s$) then gives a self-consistency equation for $\bar{\mathbf{G}}(z)$. The solution of this problem is aided by noting that equation (12) for an n-level system is analogous to the Ornstein–Zernike (OZ) equation of liquid-state theory for an n-component mixture (see, e.g., Hansen and McDonald 1986):

$$\mathbf{h}(12) = \mathbf{c}(12) + \int \mathrm{d}(3)\mathbf{h}(13)\boldsymbol{\rho}\mathbf{c}(32). \tag{38}$$

$\mathbf{h}(12)$ ($\mathbf{c}(12)$) is an $n \times n$ matrix whose (α, β) element is the total (direct) correlation function between species α and β; $\boldsymbol{\rho}$ is a diagonal $n \times n$ matrix whose (α, α) element gives the number density of species α. The parallel would be exact, with $\mathbf{H}(12)$ replacing $\mathbf{h}(12)$, $\mathbf{C}(12)$ replacing $\mathbf{c}(12)$ and $\rho\bar{\mathbf{G}}(z)$ replacing $\boldsymbol{\rho}$, except that $\bar{\mathbf{G}}(z)$, unlike $\boldsymbol{\rho}$, is not diagonal. It turns out, however, that all the liquid-state results we use rely only on $\boldsymbol{\rho}$ being symmetric, a condition that $\bar{\mathbf{G}}(z)$ also satisfies. There is a large literature devoted to solving (38) with a suitable closure condition, suggesting thereby that we may be able to solve equations (12) and (28) by exploiting the work in conventional liquid-state theory.

In fact, as shown in II for the one-level problem, this is straightforward if we use the simple step function $g_2(R)$ of equation (23) to describe correlation between site positions, in which case the closure relation (28) reduces to

$$\mathbf{H}_s(R) = 0 \qquad R < \sigma \tag{39a}$$

$$\mathbf{C}_s(R) = \mathbf{V}(R) \qquad R > \sigma. \tag{39b}$$

Within the Kirkwood superposition approximation, and for any choice of $g_2(R)$ which vanishes inside a hard core, equation (39a) is exact since each $H_s^{\alpha\beta}(R)$ will always contain a factor $g_2(R)$; the essential approximation in this model is thus equation (39b). With the above choice for $g_2(R)$, and hence equations (39), one sees directly a similarity between the SSCA/EMA equations and those relating to the mean spherical approximation (MSA) of liquid-state theory (Lebowitz and Percus 1966) which, for an n-component mixture, consist of equation (38) and the following closure conditions:

$$h^{\alpha\beta}(R) = -1 \qquad R < \sigma_{\alpha\beta} \tag{40a}$$

$$c^{\alpha\beta}(R) = -\beta\Phi^{\alpha\beta}(R) \qquad R > \sigma_{\alpha\beta}. \tag{40b}$$

Here, $\Phi^{\alpha\beta}(R)$ is the interaction potential between molecules of species α and β outside the hard core, and $\sigma_{\alpha\beta} = \frac{1}{2}(\sigma_\alpha + \sigma_\beta)$ where σ_α is the hard-sphere diameter associated with species α. The MSA for a mixture has been solved by Blum and Høye (1978) for the case where $\Phi^{\alpha\beta}(R)$ is of Yukawa form with a species-dependent pre-exponential factor (see also appendix A of Arrieta *et al* (1987) for typographical corrections). The solution has been simplified and extended by Blum (1980) and Cummings (1980).

The MSA closure equations (40) are obviously similar to those of the SSCA/EMA with a step function $g_2(R)$, equations (39). Thus, if we choose a set of Yukawa transfer matrix elements of the form (22), we ought to be able to modify the existing MSA solutions to

give a solution to the present problem. To this end we note two differences between the MSA and the current problem. First, in equations (40) the hard-core diameter $\sigma_{\alpha\beta}$ is species dependent, whereas in equation (39) σ is independent of the levels involved. Second, although equations (39*b*) and (40*b*) are formally equivalent, with $V^{\alpha\beta}(R) \leftrightarrow -\beta\Phi^{\alpha\beta}(R)$, equations (39*a*) and (40*a*) are slightly different. As mentioned in II, however, the solution of the MSA with the hard-core condition, equation (40*a*), replaced by $h^{\alpha\beta}(R) = 0$ for $R < \sigma_{\alpha\beta}$ is simpler. Because of these differences, and the previously mentioned difference between the symmetric $\bar{\mathbf{G}}(z)$ of the SSCA/EMA and the diagonal $\boldsymbol{\rho}$ of the MSA, we will summarise the method of solution. As for the MTA, we study the Yukawa matrix elements (22) such that $\alpha^{\alpha\beta} = \alpha$ for all superscripts α and β. With appropriate modifications we can therefore follow the MSA solution of Blum and Høye (1978).

The first step is a generalisation of the Wiener–Hopf factorisation technique introduced by Baxter (1968). Following Baxter (1970) and Hiroike and Fukui (1970), the OZ analogue, equation (12), can be written for $R > 0$ as

$$2\pi R\mathbf{C}_s(R) = -\mathbf{Q}'(R) + \rho\int_0^\infty \mathrm{d}R'\,\mathbf{Q}'(R'+R)\bar{\mathbf{G}}(z)\mathbf{Q}^{\mathrm{T}}(R') \tag{41a}$$

$$2\pi R\mathbf{H}_s(R) = -\mathbf{Q}'(R) + 2\pi\rho\int_0^\infty \mathrm{d}R'(R-R')\mathbf{H}_s(|R-R'|)\bar{\mathbf{G}}(z)\mathbf{Q}(R'). \tag{41b}$$

$\mathbf{Q}(R)$ is a non-symmetric matrix function, which is zero for $R < 0$ and continuous for $R > 0$; $\mathbf{Q}'(R)$ and $\mathbf{Q}^{\mathrm{T}}(R)$ are its derivative and transpose respectively. Note that we take the Baxter (1970) range parameters, beyond which the direct correlation functions vanish, to be infinite. For the Yukawa transfer matrix elements we have chosen, it can be shown that $\mathbf{Q}(R)$ must have the form

$$\mathbf{Q}(R) = \begin{cases} \mathbf{D}\,\mathrm{e}^{-\alpha R} + \mathbf{E}(\mathrm{e}^{-\alpha R} - \mathrm{e}^{-\alpha\sigma}) & R < \sigma \\ \mathbf{D}\,\mathrm{e}^{-\alpha R} & R > \sigma. \end{cases} \tag{42}$$

The problem is therefore to determine the coefficients $\mathbf{D}$ and $\mathbf{E}$, equations for which can be generated by applying the closure conditions (39) to equations (41).

If we consider equation (41*b*) for $R < \sigma$, then using equations (42) and (39*a*) we find

$$-\mathbf{E} = [\mathbf{I} - (2\pi\rho/\alpha)\hat{\mathbf{h}}(\alpha)\bar{\mathbf{G}}(z)]\mathbf{D} \tag{43}$$

where

$$\hat{\mathbf{h}}(\alpha) = \int_0^\infty \mathrm{d}R\,\mathrm{e}^{-\alpha R}\,R\mathbf{H}_s(R) \tag{44}$$

is the Laplace transform of $R\mathbf{H}_s(R)$. Next, consider equation (41*b*) for $R > \sigma$. If we subtract equation (43) from this (we are effectively using an analytic continuation of (41*b*) for $R < \sigma$ to the case $R > \sigma$) and take the Laplace transform of the resulting equation, we get

$$2\pi\hat{\mathbf{h}}(\alpha)\,(\mathbf{I} - \rho\bar{\mathbf{G}}(z)\hat{\mathbf{q}}(\alpha)) = -\tfrac{1}{2}\,\mathrm{e}^{-2\alpha\sigma}\mathbf{E} \tag{45}$$

where:

$$\hat{\mathbf{q}}(\alpha) = \int_0^\infty \mathrm{d}R\, \mathrm{e}^{-\alpha R}\mathbf{Q}(R) = [\mathbf{D} + (1 - \mathrm{e}^{-\alpha\sigma})^2\mathbf{E}]/2\alpha. \tag{46}$$

Finally, using (39*b*), equation (41*a*) for $R > \sigma$ yields

$$-(2\pi V_0/\alpha)\mathbf{a} = \mathbf{D}(\mathbf{I} - \rho\bar{\mathbf{G}}(z)\hat{\mathbf{q}}^{\mathrm{T}}(\alpha)). \tag{47}$$

Equations (43), (45) and (47) are essentially equivalent to equations (27), (33) and (29) of the Blum and Høye (1978) thermodynamic MSA; equation (45) differs slightly because of the difference between the closure conditions (39*a*) and (40*a*). These equations are in principle sufficient to determine the three unknowns $\mathbf{D}$, $\mathbf{E}$ and $\hat{\mathbf{h}}(\alpha)$ as functions of $\bar{\mathbf{G}}(z)$. The numerical solution of the equations is still, however, a non-trivial problem (see, e.g., Giunta *et al* 1985, Arrieta *et al* 1987) and further manipulations are necessary to render the problem computationally tractable.

First, note from equations (13), (16), (22) and (44) that we have

$$\begin{aligned}\mathbf{S}(z) &= -4\pi\rho V_0\mathbf{a}\bar{\mathbf{G}}(z)\int_0^\infty \mathrm{d}R\, \mathrm{e}^{-\alpha R}R\mathbf{H}_s(R) \\ &= -4\pi\rho V_0\mathbf{a}\bar{\mathbf{G}}(z)\,\hat{\mathbf{h}}(\alpha).\end{aligned} \tag{48}$$

If now we substitute for $\hat{\mathbf{q}}(\alpha)$ from equation (46), $\mathbf{E}$ from (43) and $\hat{\mathbf{h}}(\alpha)$ from (48), we find after some rearrangement that equation (45) gives

$$\left(\frac{(1 - \mathrm{e}^{-\alpha\sigma})^2}{4\alpha V_0}\mathbf{S}(z)\mathbf{a}^{-1}\mathbf{S}(z)\bar{\mathbf{G}}(z) - \mathrm{e}^{-\alpha\sigma}(1 - \mathrm{e}^{-\alpha\sigma})\mathbf{S}(z)\bar{\mathbf{G}}(z) + \alpha V_0\,\mathrm{e}^{-2\alpha\sigma}\mathbf{a}\bar{\mathbf{G}}(z)\right)\mathbf{D}$$
$$= -(\alpha/\rho)\,\mathbf{S}(z) \tag{49}$$

and, similarly, (47) gives

$$\left(\rho\frac{(1 - \mathrm{e}^{-\alpha\sigma})^2}{4\alpha V_0}\mathbf{D}^{\mathrm{T}}\mathbf{a}^{-1}\right)\mathbf{S}(z) = \rho\,\mathrm{e}^{-\alpha\sigma}(1 - \tfrac{1}{2}\mathrm{e}^{-\alpha\sigma})\mathbf{D}^{\mathrm{T}} - \alpha\bar{\mathbf{G}}^{-1}(z)$$
$$- 2\pi V_0\bar{\mathbf{G}}^{-1}(z)\mathbf{D}^{-1}\mathbf{a}. \tag{50}$$

In manipulating and simplifying these and the following equations it is helpful to remember that $\bar{\mathbf{G}}(z)$, $\hat{\mathbf{h}}(\alpha)$, $\mathbf{a}$, $\mathbf{S}(z)$ and $\mathbf{z}$ are symmetric matrices. Moreover it follows from equation (48) that the matrix product $\mathbf{S}(z)\bar{\mathbf{G}}(z)\mathbf{a}$ is symmetric and hence $\mathbf{S}(z)\bar{\mathbf{G}}(z)\mathbf{a} = \mathbf{a}\bar{\mathbf{G}}(z)\mathbf{S}(z)$. Other useful results follow from this; if, for example, we substitute for $\mathbf{S}(z)$ from equation (16), then we find that $\mathbf{z}\bar{\mathbf{G}}(z)\mathbf{a} = \mathbf{a}\bar{\mathbf{G}}(z)\mathbf{z}$. It is now convenient to introduce the reduced variables defined in equations (24) and (25). If we also define $\mathbf{D}^* = \mathbf{D}/V_0^*\sigma^2$ then equations (49) and (50) may be rewritten as

$$\left(\frac{(1 - \mathrm{e}^{-\tilde{\alpha}})^2}{4\tilde{\alpha}}\tilde{\mathbf{S}}(z)\mathbf{a}^{-1}\tilde{\mathbf{S}}(z)\tilde{\mathbf{G}}(z) - \mathrm{e}^{-\tilde{\alpha}}(1 - \mathrm{e}^{-\tilde{\alpha}})\tilde{\mathbf{S}}(z)\tilde{\mathbf{G}}(z) + \tilde{\alpha}\,\mathrm{e}^{-2\tilde{\alpha}}\mathbf{a}\tilde{\mathbf{G}}(z)\right)\mathbf{D}^*$$
$$= -(\tilde{\alpha}/\rho^*)\tilde{\mathbf{S}}(z) \tag{51}$$

and

$$\left(\rho^*\frac{(1 - \mathrm{e}^{-\tilde{\alpha}})^2}{4\tilde{\alpha}}\mathbf{D}^{*\mathrm{T}}\mathbf{a}^{-1}\right)\tilde{\mathbf{S}}(z) = \rho^*\,\mathrm{e}^{-\tilde{\alpha}}(1 - \tfrac{1}{2}\mathrm{e}^{-\tilde{\alpha}})\mathbf{D}^{*\mathrm{T}} - \tilde{\alpha}\tilde{\mathbf{G}}^{-1}(z)$$
$$- 2\pi\tilde{\mathbf{G}}^{-1}(z)\mathbf{D}^{*\,-1}\mathbf{a}. \tag{52}$$

It can be seen that equation (51) ((52)) is linear in $\mathbf{D}^*$ ($\tilde{\mathbf{S}}(z)$). One way to exploit the linearity would be to iterate equations (51) and (52), using the former to find $\mathbf{D}^*$ as a function of $\tilde{\mathbf{S}}(z)$ and $\tilde{\mathbf{G}}(z)$, and the latter to find $\tilde{\mathbf{S}}(z)$ as a function of $\mathbf{D}^*$ and $\tilde{\mathbf{G}}(z)$. Convergence of this iteration would yield $\tilde{\mathbf{S}}(z)$ as a function of $\tilde{\mathbf{G}}(z)$ only; and iteration of this solution together with equation (16) would then give $\mathbf{G}(z)$. We find, however, that the iteration of equations (51) and (52) is highly unstable, in agreement with the conclusion of Arrieta *et al* (1987) for the normal MSA problem that it is not practicable to use the linearity mentioned above. We must therefore treat equations (51) and (52) as simultaneous non-linear equations.

The problem may be simplified by incorporating equation (16) directly into equations (51) and (52). This can be done by writing (16) in reduced form as $\tilde{\mathbf{S}}(z) = \tilde{\mathbf{z}} - \tilde{\mathbf{G}}^{-1}(z)$, and employing this in equations (51) and (52) to give

$$\mathbf{0} = \frac{(1-\mathrm{e}^{-\tilde{\alpha}})^2}{4\tilde{\alpha}}\tilde{\mathbf{z}}\mathbf{a}^{-1}(\tilde{\mathbf{z}}\tilde{\mathbf{G}}(z) - 2\mathbf{I} + \tilde{\mathbf{G}}^{-1}(z)\tilde{\mathbf{z}}^{-1}) - \mathrm{e}^{-\tilde{\alpha}}(1-\mathrm{e}^{-\tilde{\alpha}})(\tilde{\mathbf{z}}\tilde{\mathbf{G}}(z) - \mathbf{I})$$

$$+ \tilde{\alpha}\,\mathrm{e}^{-2\tilde{\alpha}}\mathbf{a}\hat{\mathbf{G}}(z) + (\tilde{\alpha}/\rho^*)(\tilde{\mathbf{z}} - \hat{\mathbf{G}}^{-1}(z))\mathbf{D}^{*-1} \tag{53}$$

and:

$$\mathbf{0} = \frac{\rho^*(1-\mathrm{e}^{-\tilde{\alpha}})^2}{4\tilde{\alpha}}\mathbf{D}^{*\mathrm{T}}\mathbf{a}^{-1}(\tilde{\mathbf{z}}\tilde{\mathbf{G}}(z) - \mathbf{I}) - \rho^*\,\mathrm{e}^{-\tilde{\alpha}}(1 - \tfrac{1}{2}\mathrm{e}^{-\tilde{\alpha}})\mathbf{D}^{*\mathrm{T}}\tilde{\mathbf{G}}(z)$$

$$+ \tilde{\alpha}\mathbf{I} + 2\pi\tilde{\mathbf{G}}^{-1}(z)\mathbf{D}^{*-1}\mathbf{a}\tilde{\mathbf{G}}(z). \tag{54}$$

Equations (53) and (54) may be solved by a Newton–Raphson technique to yield $\tilde{\mathbf{G}}(z)$ and $\mathbf{D}^*$; equation (25) then gives the reduced DOS. These equations will clearly produce a multiplicity of solutions, and it is necessary to choose the physically correct one (see, e.g., Pastore (1988) for the analogue of this problem in the thermodynamic MSA context). Location of the correct root is aided by comparison with that for a known limit, such as $a^{\alpha\beta} = a$ for all α, β, the case of identical $V^{\alpha\beta}(R)$ described in § 3, or $a^{01} = 0 = a^{10}$ in which case the problem separates into two uncoupled one-level problems, or $\sigma = 0$ in which case we have the MTA limit. Another check on the acceptability of a root is that the resultant total DOS be correctly normalised to two. Whether or not the correct root is located is highly influenced by the initial estimate used in the Newton–Raphson algorithm. To produce a reliable initial input it is sensible to proceed, stepwise, from a known limit; we have chosen to use the $a^{01} = 0$ limit, from which we successively increase the a^{01} interlevel coupling.

In figures 6–8 we plot $\tilde{D}_0(e)$ (broken curve), $\tilde{D}_1(\varepsilon)$ (dotted curve) and the total DOS $\tilde{D}_0(\varepsilon) + \tilde{D}_1(\varepsilon)$ (full curve) for a variety of different parameters. In figure 6 we consider a fixed density $\rho^* = 0.1$, $\Delta\varepsilon = 1$, $\tilde{\alpha} = 0.8$, $a^{00} = 0.7$ and $a^{11} = 1$, and we investigate the effect of band coupling by taking two different values of a^{01}, namely $a^{01} = 0.55$ (spectrum A) and 0.7 (spectrum B). Both these spectra, but especially A, retain remnant features of the uncoupled bands, with the characteristic asymmetry and long low-energy subband tails. As before, though, the coupling implicit in a^{01} causes mixing throughout the bands except at the zero-order energies, and introduces a repulsion between the subbands which leads to the outer band edges moving further outward and the production

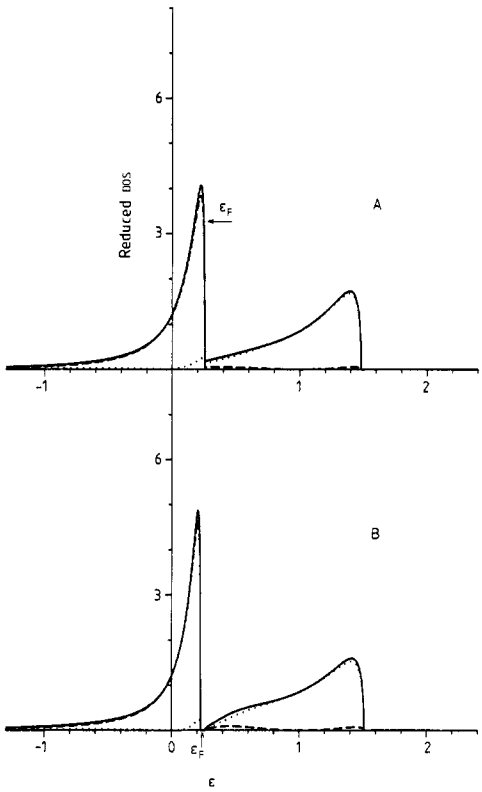

Figure 6. $\tilde{D}_0(\varepsilon)$ (broken curve), $\tilde{D}_1(\varepsilon)$ (dotted curve) and $\tilde{D}_0(\varepsilon) + \tilde{D}_1(\varepsilon)$ (full curve) in the SSCA/EMA for $\rho^* = 0.1$, $\Delta\varepsilon = 1$, $\tilde{\alpha} = 0.8$, $a^{00} = 0.7$, $a^{11} = 1$ and (A) $a^{01} = 0.55$, (B) $a^{01} = 0.7$. Note the change in scale on the DOS axis from that used in figures 2–4.

of a band gap at $a^{01} = 0.7$ (spectrum B). Computer simulations for the one-level per site case (Bush *et al* 1989a) show that the lower limit of applicability of the SSCA/EMA (with a step function $g_2(R)$) is $\rho^* \simeq 0.1$. This choice does, however, allow a quantitative comparison with the Hubbard DOS if we note that spectra A and B of figure 6 have the same parameters as for spectra B of figure 3 and C of figure 2 respectively. We see that the results from the two theories differ greatly, the principal differences arising from the inherent asymmetry in the SSCA/EMA bands; computer simulations on the model system show that the SSCA/EMA reproduces the essential features much more adequately than the Hubbard level of description (Bush *et al* 1989b). Despite this, however, and for the parameters specified above, the band gap appears at a similar value of $a^{01}: a^{01} \simeq 0.6$ for the Hubbard theory and $a^{01} \simeq 0.7$ for the SSCA/EMA.

In agreement with the MTA, and in contrast to Hubbard, we find that the $n = 1$ Fermi energy is blue shifted slightly to positive energies. Further, on increasing a^{01}, ε_F increases, as too do $\tilde{D}_1(\varepsilon_F)$ and the total DOS at ε_F. As with the MTA, therefore, we see that an excited level can have an appreciable effect on the nature of Fermi level states for a half-filled valence band. The $n = 2$ Fermi energy is marked on figures 6–8. As before, ε_F lies in the band gap whenever it exists: such is the case for spectrum B in figure 6 and thus the system is insulating. On decreasing a^{01} the band gap closes (see spectrum A of figure 6), initially forming a (probably localised) pseudogap around ε_F until, on decreasing a^{01} further, ε_F moves out of the pseudogap leading ultimately to an Anderson insulator–metal transition.

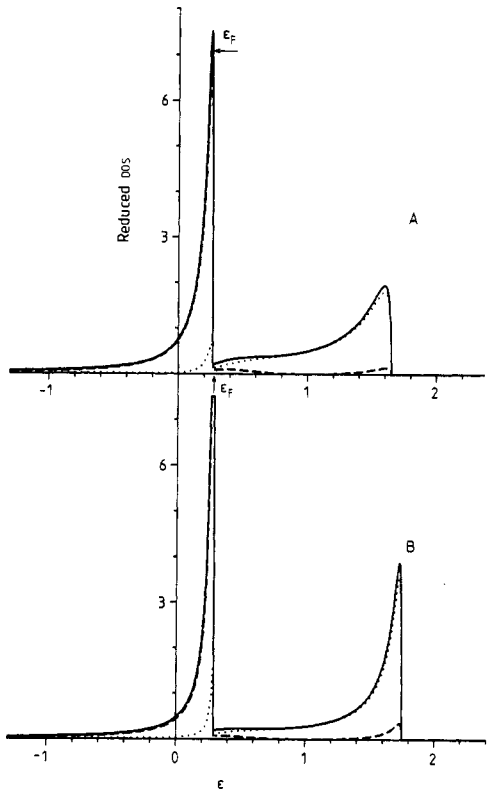

Figure 7. As figure 6 but with a fixed $a^{01} = 0.7$ and (A) $\rho^* = 0.3$, (B) $\rho^* = 1$. In spectrum B the total reduced DOS peaks at 17.

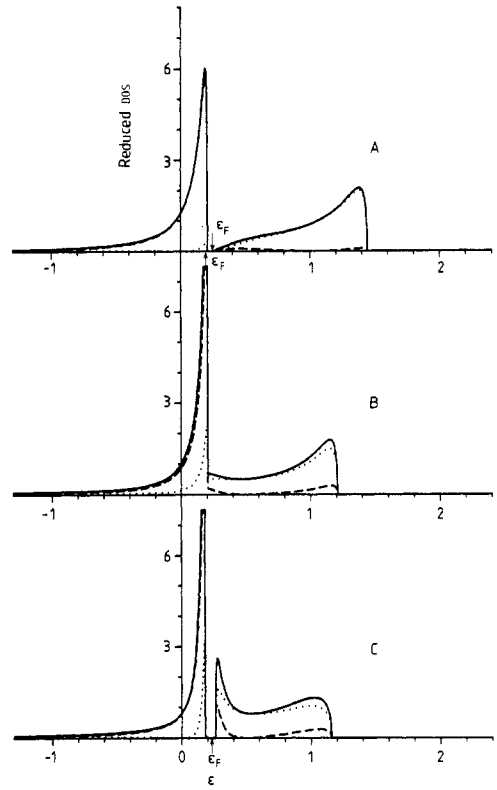

Figure 8. As figure 6 but with a fixed $a^{01} = 0.7$ and (A) $\rho^* = 0.3$, $\tilde{a} = 1.2$, (B) $\rho^* = 0.3$, $\Delta\varepsilon = 0.5$, and (C) $\rho^* = 0.3$, $\Delta\varepsilon = 0.5$, $a^{11} = 0.7$. In spectrum B (C) the total reduced DOS peaks at 12 (14).

In figure 7 we examine the evolution of a pseudogap consequent upon a change in ρ^*, using the same parameters as in spectrum B of figure 6, except that ρ^* is increased to $\rho^* = 0.3$ (spectrum A) and then to $\rho^* = 1$ (spectrum B). In going from spectrum B of figure 6 to A of figure 7 we see that the density increase causes sufficient broadening of the sub-bands to close the band gap, but in going from spectrum A of figure 7 ($\rho^* = 0.3$) to spectrum B ($\rho^* = 1$) there is little qualitative change; in particular the pseudogap essentially persists over the entire density range. As discussed previously, however, what is important is the position of ε_F in relation to the pseudogap rather than the existence of the pseudogap itself. As ρ^* increases, both the minimum in the total DOS and ε_F (for $n = 2$) move to progressively higher energies, but the latter increases less, so that ε_F effectively moves towards the maximum in the total DOS and will eventually cross a mobility edge into a region of delocalised states, resulting in a disorder-induced insulator–metal transition. This behaviour is evident in figure 7 where, for $\rho^* = 0.3$ (spectrum A), $\varepsilon_F = 0.259$ lies midway between the maximum (at $\varepsilon = 0.253$) and minimum (at $\varepsilon = 0.265$) in the total DOS, with $\tilde{D}_0(\varepsilon_F) + \tilde{D}_1(\varepsilon_F) = 7.0$ somewhat less than the maximum value (7.5) of the total DOS; in spectrum B, where $\rho^* = 1$, $\varepsilon_F = 0.283$ is essentially coincident with the maximum in the total DOS, $\tilde{D}_0(\varepsilon_F) + \tilde{D}_1(\varepsilon_F) = 16.5$.

In figure 8 we show the effect of varying some of the other physically relevant parameters. Spectrum A has the same parameters as in spectrum A of figure 7, except

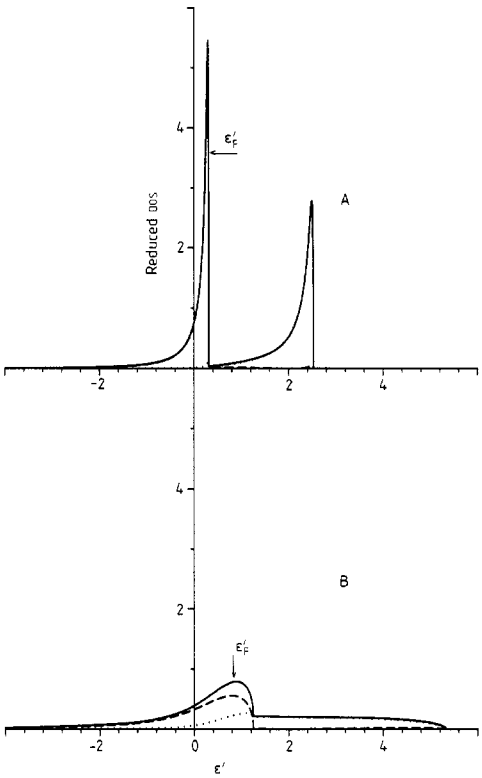

Figure 9. (A) $D'_0(\varepsilon')$ (broken curve), $D'_1(\varepsilon')$ (dotted curve) and $D'_0(\varepsilon') + D'_1(\varepsilon')$ (full curve) in the SSCA/EMA for $\rho' = 0.5$, $\Delta\varepsilon' = 2$, $\tilde{\alpha} = 0.5$, $a^{00} = 0.7$, $a^{01} = 0.55$ and $a^{11} = 1$ compared with (B) the perfectly random limit result ($\tilde{\alpha} = 0$) obtained from the MTA for $\rho' = 0.5$, $\Delta\varepsilon' = 2$, $a^{00} = 0.7$, $a^{01} = 0.55$ and $a^{11} = 1$. Note the different set of units used from those used in figures 2–4 and 6–8, and the change in scale from that used in figure 5.

that we decrease the range of all the transfer matrix elements by increasing $\tilde{\alpha}$ to 1.2. This has the effect of narrowing the sub-bands sufficiently to create a band gap, the system thus being insulating for $n = 2$. In spectrum B we again use the parameters of spectrum A of figure 7, but now we decrease the zeroth-order energy gap to $\Delta\varepsilon = 0.5$. This naturally results in greater overlap between the two sub-bands and hence a build up in the total DOS about its sharp maximum value. Moreover the greater overlap increases the number of states in the lower sub-band, so that for $n = 2$, ε_F is at a slightly lower energy than the maximum in the DOS. In spectrum C we take the parameters of spectrum B, but reduce a^{11} from 1 to 0.7. This reduces the width of the upper sub-band and creates a band gap, which is to be expected since we now have the case of identical transfer matrix elements described in § 3. In addition, the normal asymmetry of the upper band is reversed to give a shape more characteristic of that resulting from the Hubbard level of approximation.

In figure 9 we compare quantitatively the SSCA/EMA with a step function $g_2(R)$, and the MTA to which the former reduces in the limit $\sigma = 0$. To do this we use the following expressions to interrelate the relevant variables in the two theories:

$$\rho' = \rho^* \tilde{\alpha}^{-3} \qquad \Delta\varepsilon' = \Delta\varepsilon\tilde{\alpha}^{-1} \qquad \varepsilon' = \varepsilon\tilde{\alpha}^{-1} \qquad D'_\alpha(\varepsilon') = \tilde{\alpha}\tilde{D}_\alpha(\varepsilon). \tag{55}$$

Spectrum A is the SSCA/EMA result for $\rho' = 0.5$, $\Delta\varepsilon' = 2$, $\tilde{\alpha} = 1$, $a^{00} = 0.7$, $a^{01} = 0.55$ and $a^{11} = 1$, corresponding to $\rho^* = 0.5$ and $\Delta\varepsilon = 2$; spectrum B is the MTA result corresponding to the same parameters except for $\tilde{\alpha}$, which is zero. The sole difference in

going from B to A is thus the inclusion of a hard-sphere diameter σ, here set equal to the effective Bohr radius, $a_H \equiv \alpha^{-1}$. We see that this has a dramatic effect on the DOS, and in liquid metals that are adequately described by a tight-binding model we indeed expect to have $\tilde{\alpha} \sim 1$: it is clear in these cases that the MTA is liable to produce a grossly inaccurate description of the DOS.

6. Site-diagonal disorder

Finally, we comment briefly on the incorporation of site-diagonal disorder into any single-site theory for the averaged Green functions. As mentioned in § 2, the ε_{i_α} of equation (1) may be regarded as independent random variables in the site index, with a given probability distribution $P(\varepsilon_{i_0}, \varepsilon_{i_1})$ which is the same for each site. This problem has been discussed in detail in I for a one-level system. There, by considering the diagonal and off-diagonal averaged Green functions in which the site energies associated with the root points are constrained to specific values, a self-consistency equation was derived for the one-level $\bar{G}(z)$ (averaged over all configurations and site energies) which incorporates $P(\varepsilon_i)$ and is valid for any single-site theory. For a two-level system, if we consider $\bar{G}^{\alpha\beta}(z)$ and $\bar{G}^{\alpha\beta}(12)$ in which the zero-order site energies of both levels associated with each root point are fixed, we arrive at the following generalisation of the result derived in I:

$$\bar{\mathbf{G}}(z) = \int_{-\infty}^{\infty} \mathrm{d}\varepsilon_{i_0} \int_{-\infty}^{\infty} \mathrm{d}\varepsilon_{i_1}\, P(\varepsilon_{i_0}, \varepsilon_{i_1})(\mathbf{z}_i - \mathbf{S}(z))^{-1}. \tag{56}$$

Here, $\mathbf{z}_i$ has the non-zero elements $(\mathbf{z}_i)^{00} = z - \varepsilon_{i_0}$ and $(\mathbf{z}_i)^{11} = z - \varepsilon_{i_1}$; $\mathbf{S}(z) \equiv \mathbf{S}(\bar{\mathbf{G}}(z))$ is the single-site self-energy which is *independent* of ε_{i_0} and ε_{i_1} and which, viewed as a function of $\bar{\mathbf{G}}(z)$, is identical to the (known) self-energy in the *absence* of site-diagonal disorder. Equation (56) thus provides a simple and practicable self-consistency equation for $\bar{\mathbf{G}}(z)$ averaged over all configurations and site energies. Knowledge of $\mathbf{S}(z)$ as a function of $\bar{\mathbf{G}}(z)$ for the case where diagonal disorder is absent (e.g., from equations (35), or (51) and (52)) is all that is required for an explicit evaluation of $\bar{\mathbf{G}}(z)$, and hence the DOS, when both topological and site-diagonal disorder are present.

Acknowledgments

MDW is grateful to the SERC for the award of a postgraduate studentship, and DEL thanks the British Petroleum Venture Research Unit for their support.

References

Arrieta E, Jedrzejek C and Marsh K N 1987 *J. Chem. Phys.* **86** 3607–26
Baxter R J 1968 *Aust. J. Phys.* **21** 563–9
—— 1970 *J. Chem. Phys.* **52** 4559–62
Blum L 1980 *J. Stat. Phys.* **22** 661–72
Blum L and Høye J S 1978 *J. Stat. Phys.* **19** 317–24
Bush I J, Logan D E, Madden P A and Winn M D 1989a *J. Phys.: Condens. Matter* **1** 2551–5
—— 1989b *J. Phys.: Condens. Matter* **1** 8735–9
Cummings P T 1980 *PhD thesis* University of Melbourne

Figueira M S, Makler S S and Anda E V 1984 *J. Phys. C: Solid State Phys.* **17** 623–36
Giunta G, Abramo M C and Caccamo C 1985 *Mol. Phys.* **56** 319–33
Hansen J-P and McDonald I R 1986 *Theory of Simple Liquids* (New York: Academic)
Hiroike K and Fukui Y 1970 *Prog. Theor. Phys.* **43** 660–71
Hubbard J 1963 *Proc. R. Soc.* A **276** 238–57
—— 1964 *Proc. R. Soc.* A **281** 401–19
Ishida Y and Yonezawa F 1973 *Prog. Theor. Phys.* **49** 731–53
Lebowitz J L and Percus J K 1966 *Phys. Rev.* **144** 251–8
Logan D E and Winn M D 1988 *J. Phys. C: Solid State Phys.* **21** 5773–95
Matsubara T and Toyazawa Y 1961 *Prog. Theor. Phys.* **26** 739–56
Movaghar B and Miller D E 1975 *J. Phys. F: Metal Phys.* **5** 261–77
Pastore G 1988 *Mol. Phys.* **63** 731–41
Roth L M 1974 *J. Physique* **35** C4 317–23
—— 1976 *J. Phys. F: Metal Phys.* **6** 2267–88
Stratt R M and Xu B-C 1989a *Phys. Rev. Lett.* **62** 1675–8
—— 1989b *J. Chem. Phys.* submitted
Wertheim M S 1973 *Mol. Phys.* **25** 211–23
Winn M D and Logan D E 1989 *J. Phys.: Condens. Matter* **1** 1753–71
Yonezawa F, Ishida Y, Martino F and Asano S 1977 *Liquid Metals 1976* (Inst. Phys. Conf. Ser. No 30) (Bristol and London: The Institute of Physics) pp 385–97
Yonezawa F and Martino F 1976 *J. Phys. F: Metal Phys.* **6** 739–47